




# CHAPTER 5 RESEARCH ON THE MOON AND MARS


**Research on the Moon and Mars**

by Bob Silberg, Raytheon

Jack Sandweiss of Yale University discussed the search for particles of strange quark matter (SQM or "strangelets"), which are thought to be torn from neutron stars (which may actually be strange-quark stars) by the tidal forces of a binary. While primarily an issue of basic science, he speculated that such material might be useful for spacecraft propulsion.

Vigdor Teplitz of the Goddard Space Flight Center described the seismic search for strangelets. A micron-size particle weighing about a ton would likely plow through the Earth virtually instantaneously, setting off a distinctive pattern of seismic signals. A study of such patterns turned up a number of possible candidates. He said the Moon would be a better detector, despite its smaller radius, because of the greatly reduced background noise.

Ho Jung Paik of the University of Maryland discussed the merits of the Moon for a gravitational wave (GW) detection experiment. GWs, he pointed out, can probe the universe from $10^{-35}$ seconds after the Big Bang, much earlier than light and neutrinos. The Moon offers low background noise and free vacuum.

Robert Duncan of the University of New Mexico talked about studies of dynamical critical phenomena and complexity studies in $^{4}$He. Acknowledging that this is fundamental research, he argued that since preparations are 90% complete, it would be a shame not to do the remaining 10% and get science results. The study requires microgravity, and involves new advances in temperature control and mini-high-resolution thermometers.

David Lee of Cornell University discussed the usefulness of $^{3}$He and the possibility of mining it on the Moon. The substance is good for neutron detectors and shields, ultra-low temperature IR bolometers, superfluid gyroscopes, atom interferometers, and medical imaging of the interior of the lung. It would also be good for nuclear fusion generators. Though the data is not in hand, it might be more economical to import $^{3}$He from the Moon than to make it in reactors.

Jens Grundlach of the University of Washington spoke about tests of the Equivalence Principle using an ultra-sensitive torsion balance. He said that torsion balances are the most sensitive force sensors for macroscopic objects on the ground, and can provide a test bed for proposed experiments in space, such as comparing Moon material and Earth-core material falling towards the Sun.

Slava Turyshev of JPL discussed the Lunar Astronometric Test of Relativity (LATOR), which is described as a 21$^{st}$-century version of the Michelson-Morley experiment, designed to search for the presence of a cosmologically evolved scalar field in the solar system. It would test General Relativity to a part in $10^{8}$ by measuring three sides of a light triangle, one side of which passes close to the Sun.

Ken Nordtvedt of Northwest Analysis expanded on the LATOR theme by describing a configuration in which two sides of the triangle straddle the Sun, thereby reducing the precision needed in locating them with respect to the Sun.

# Strange Quark Matter
# Status and Prospects

2004 NASA/JPL Workshop

On

Physics for planetary Exploration

J. Sandweiss April 21, 2004

# Strange Quark Matter

Stable or metastable massive multiquark states containing u,d and s quarks.

*"Artist's Interpretation"*

Nuclear Matter
(Carbon)
Z=6
A=12
Z/A=1/2

Strange Matter
(Strangelet)
Z=1
A=12 (36 quarks)
Z/A=0.083
$N_S$=10, $f_S$=$N_S$/A=0.83

# Strange Quark Matter

The existence of quark states with more than three quarks is allowed in QCD. The stability of such quark matter states has been studied with lattice QCD and phenomenological bag models, but is not well constrained by theory.

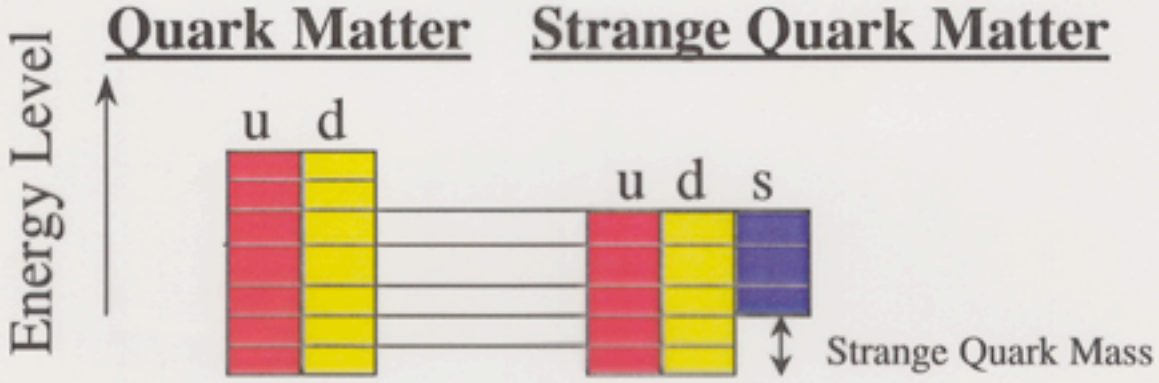


The addition of strange quarks to the system allows the quarks to be in lower energy states despite the additional mass penalty.

There is additional stability from reduced Coulomb repulsion. SQM is expected to have **low Z / A**.

From Farhi and Jaffe

**From E. Farhi and R. L. Jaffe, Phys. Rev. D 30, 2379-90 (1984).**

MIT Bag Model Calculation

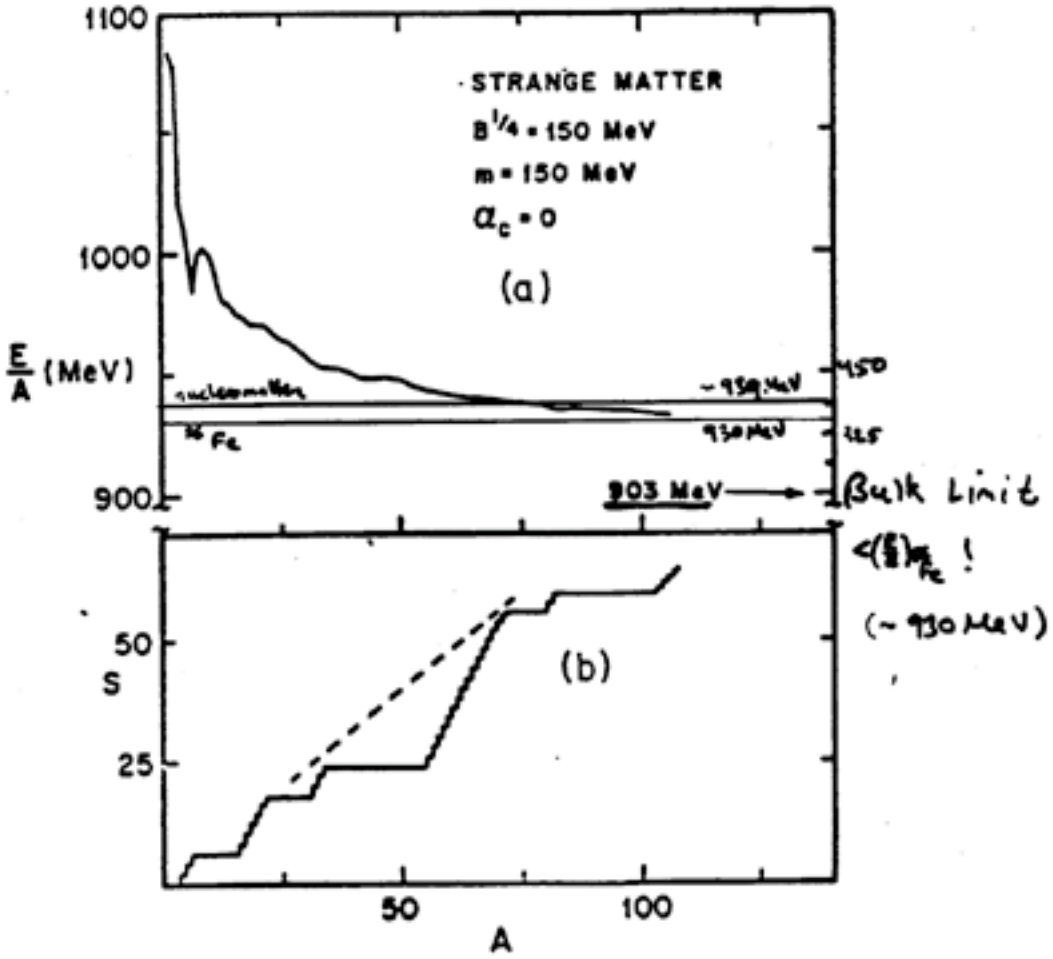


FIG. 4. (a) $E/A$ versus $A$ in the hadronic bag model for $u$, $d$, and $s$ quarks. Parameters are such that $E/A$ in bulk is 903 MeV. (b) $S$ versus $A$ in the hadronic bag model for $u$, $d$, and $s$ quarks. Parameters are such that $E/A$ in bulk is 903 MeV.

- Most stable when $\frac{S}{A} \sim 0.8$
- Becomes more stable with higher A

EXPERIMENTAL QUESTION

# Color-flavor locked strangelets

Jes Madsen
*Institute of Physics and Astronomy, University of Aarhus, DK-8000 Århus C, Denmark*
(August 3, 2001)

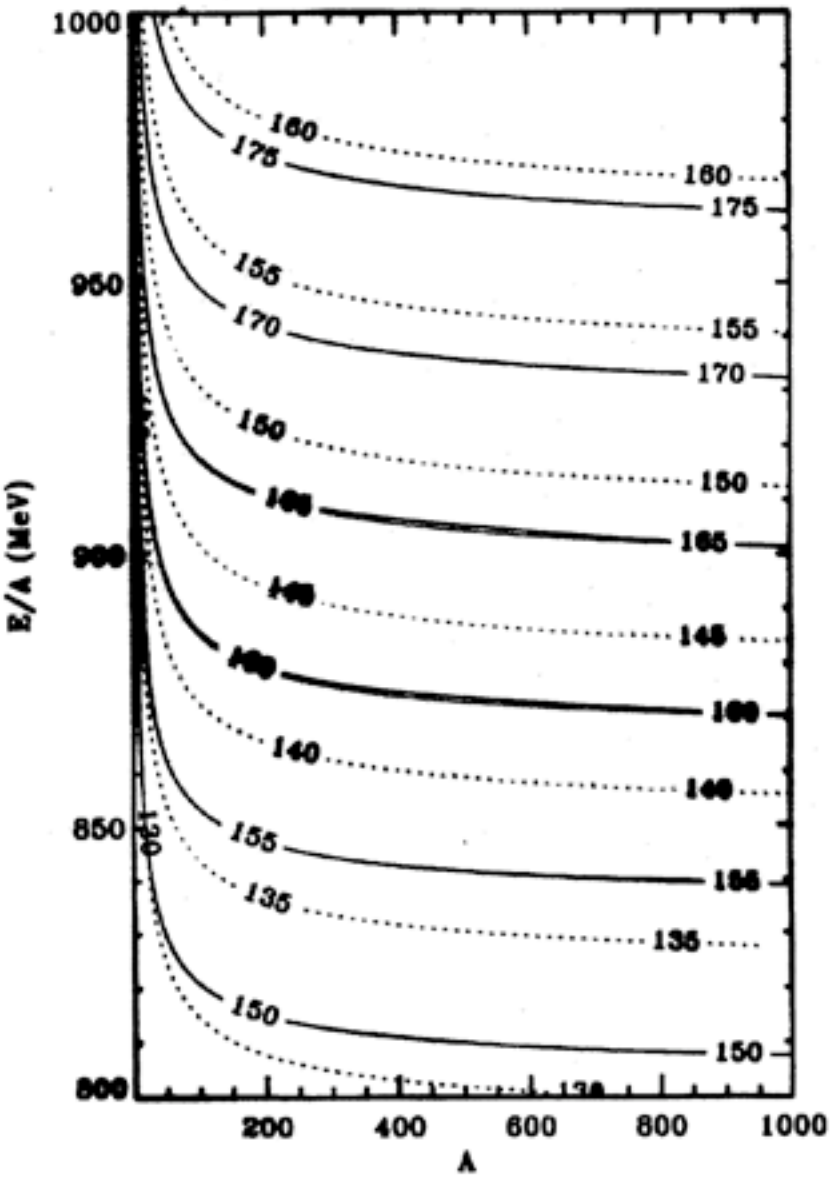


FIG. 2. Energy per baryon in MeV as a function of $A$ for CFL-strangelets (full curves) and ordinary strangelets (dashed curves) with $B^{1/4}$ in MeV as indicated, $\Delta = 100$MeV and $m_s = 150$MeV.

# CFL Charge/Mass Relation for Strangelets:

# $Z \sim 0.3\ A^{2/3}$

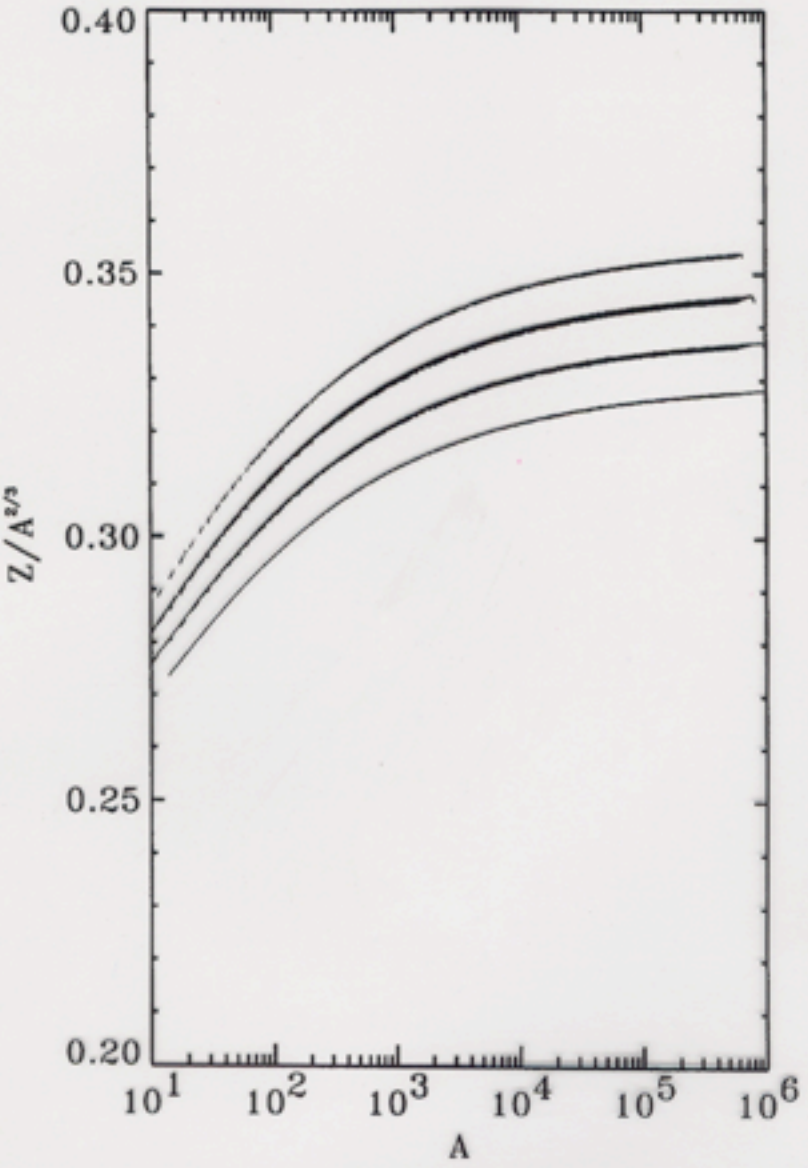


FIG. 3. Charge divided by $A^{2/3}$ as a function of $A$ for CFL-strangelets with $B^{1/4} = 150$, 160, 170, and 180 MeV (top to bottom), $\Delta = 100$MeV and $m_s = 150$MeV.

# Properties of Strangelets

The size of a strangelet is unlimited (for $A > A_{min}$)

Since strangelets have low Z/A, Coulomb energy is not important - *no fission*.

Strangelets can grow by absorbing neutrons - this is an exothermic reaction (~20MeV photon emission)

*New Energy Source*

Shaw, Shin, Dalitz, Desai, *Nature*, 337, (1989), 436.

Strangelets with $A > 10^{17}$ ($R > 5$ angstroms) cannot be supported on the surface of the earth (mg ~ 1 eV/angstrom)

"Strangelets" with $M > 2*M_{SUN}$ will collapse into a black hole.
Strange quark systems with $M < 2*M_{SUN}$ would be similar to neutron stars ("strange stars").

SQM is the true ground state of hadronic, baryonic matter.

# Properties of Strangelets (Continued)

## Atomic Z up to 1000

Because of the low charge density inside a strangelet the total charge can exist up to Z=1000 before Spontaneous pair creation shields the nuclear charge.

A new chemistry becomes available

Production of VERY dense matter

# Conclusions from Accelerator Searches

- It is not possible to make strangelets with A>8 by coalescence at accelerators

- In a region where there is evidence for making QGP, no strangelets are seen

  - No Light Metastable Strangelets Exist (A<100, $\tau$>100ns)

  - OR -

  - No QGP

  - OR -

  - No distillation mechanism

Further work at accelerators will not answer the question of the existence of stable SQM at zero pressure

beam of 450 MeV which is below the Coulomb barrier of normal matter. Gamma multiplicities and gamma total energies have been measured. If these probes would contain a substantial fraction of strange quark matter one expects either a high gamma multiplicity or a high total gamma energy. None of it was observed leading to an upper limit of strangelet concentration in these material in the order of $10^{-13}$ to $10^{-16}$ per ordinary nucleon for strangelet masses between $10^3$ and $10^8$ amu. These limits are about a factor 100 better compared to earlier measurements mentioned above which use the technique of Rutherford backscattering (Brügger *et al* 1989).

A compilation of achieved limits on the concentration relative SQM abundance is shown in figure 3 Data has been taken from the compilation by (Blackman and Jaffe 1989) and the measurements by Brügger *et al* (1989), Hemmick *et al* (1990), Vandegriff *et al* (1996) and Perillo Isaac *et al* (1998).

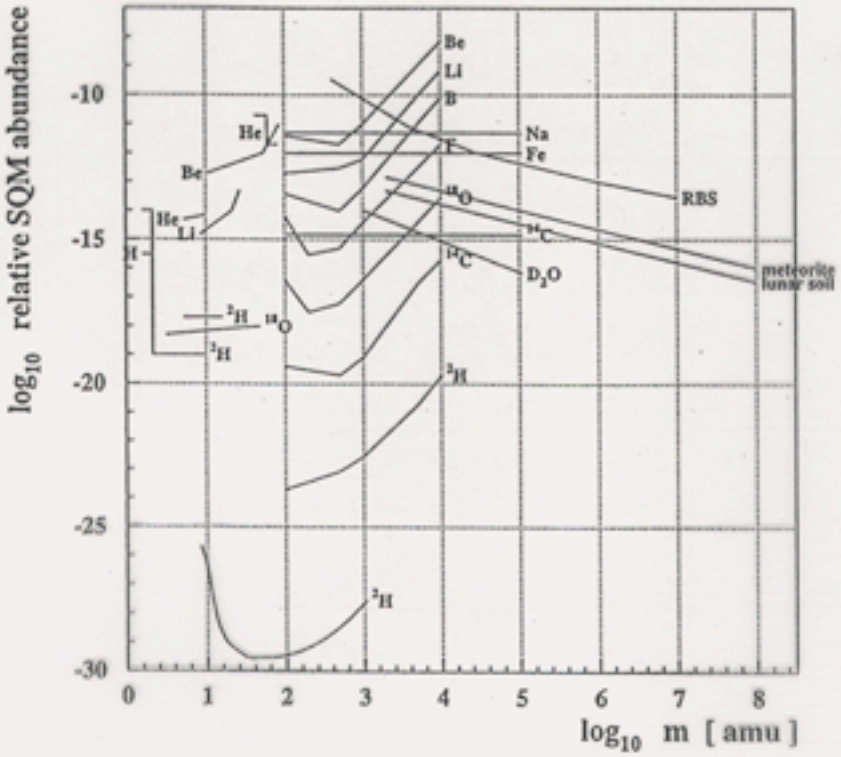


R. Klingenberg
J. Physics G25,
R 273, (1999)

R. Klingenberg, J. Physics G - Nuclear and Particle Physics 25, R273 (1999)

**Figure 3.** Upper limits on the abundance of stable strange quark matter as heavy isotopes determined in various probes as discussed in the text.

The concentration limits as found by the experimental investigation allows to set limits on the flux of SQM as nuclearites. It is based on the general assumption that galactic cosmic radiation containing stable strange quark matter is absorbed and deposited in

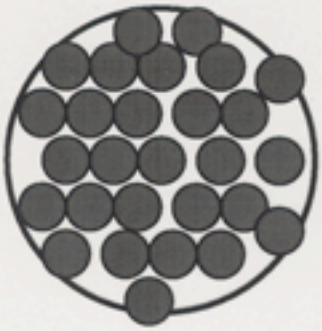

**No stable strange matter - *Neutron Stars***

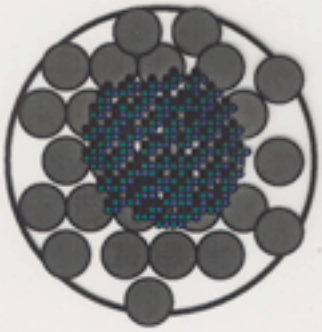

**Strange matter stable under pressure - *Hybrid Stars***

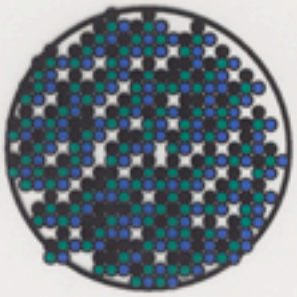

**Strange matter stable at zero pressure - *Strange Stars***

# IF Strange Quark Matter is Stable at Zero External Pressure, All Compact Stars are Strange Stars not Neutron Stars!

Contact
Steve Roy
Media Relations Department
(256) 544-0034
steve.roy@msfc.nasa.gov

Delores Beasley
NASA Headquarters
(202) 358-1753

Megan Watzke
Chandra X-ray Observatory Center
(617) 496-7998

NASA News Release
National Aeronautics and Space Administration
Marshall Space Flight Center - Huntsville, Ala. 35812
http://www.msfc.nasa.gov/news

For Release: April 10, 2002

Release: 02-082

# Cosmic X-rays reveal evidence for new form of matter

NASA's Chandra X-ray Observatory has found two stars - one too small, one too cold - that reveal cracks in our understanding of the structure of matter. These discoveries open a new window on nuclear physics, offering a link between the vast cosmos and its tiniest constituents.

Chandra?s observations of RXJ1856.5-3754 and 3C58 suggest that the matter in these stars is even denser than nuclear matter found on Earth. This raises the possibility these stars are composed of pure quarks or contain crystals of sub-nuclear particles that normally have only a fleeting existence following high-energy collisions.

By combining Chandra and Hubble Space Telescope data, astronomers found that RXJ 1856 radiates like a solid body with a temperature of 1.2 million degrees Fahrenheit (700,000 degrees Celsius) and has a diameter of about 7 miles (11.3 kilometers). This size is too small to reconcile with standard models for neutron stars - until now the most extreme form of matter known.

?Taken at face value, the combined observational evidence points to a star composed not of neutrons, but of quarks in a form know as strange quark matter,? said Jeremy Drake of the Harvard-Smithsonian Center for Astrophysics (CfA) in Cambridge, Mass., and lead author of a paper on RXJ1856 to appear in June 20, 2002 issue of The Astrophysical Journal. ?Quarks, thought to be the fundamental constituents of nuclear particles, have never been seen outside a nucleus in Earth-bound laboratories.?

Observations by Chandra of 3C58 also yielded startling results. A team composed of Patrick Slane and Steven Murray, also of CfA, and David Helfand of Columbia University, New York, failed to detect the expected X-radiation from the hot surface of 3C58, a neutron star believed to have been created in an explosion witnessed by

## The Web

The newly discovered star RXJ 1856 is too small for standard models. (NASA et al.)

Fact sheet

## E-mail

Get releases sent directly to you! Contact:
judy.pettus@msfc.nasa.gov

## Other news releases

# SQM Fragments from Colliding Strange Stars (Inspirals)

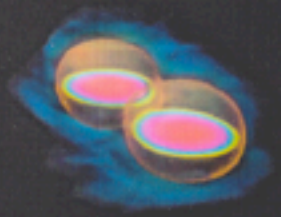

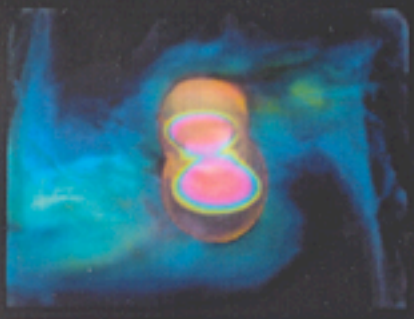

- Tidal Formation of fragments: size - $A \sim 10^{38}$
- Fragments Spend time in *figure 8* orbits, v~0.1c
- Interactions split fragments into smaller fragments and provide a mechanism to inject fragments into galaxy
- As much as 0.1 $M_{SUN}$ can be ejected.

# one Two Seismic Events with the Properties for the Passage of Strange Quark Matter Through the Earth

David P. Anderson
Department of Geological Sciences
Southern Methodist University
dpa@io.isem.smu.edu

Eugene T. Herrin
Department of Geological Sciences
Southern Methodist University
herrin@passion.isem.smu.edu

Vigdor L. Teplitz
Department of Physics
Southern Methodist University
vteplitz@ostp.eop.gov

Ileana M. Tibuleac
Weston Geophysical
Boston, MA
ileana@westongeophysical.com

## I. INTRODUCTION

In this paper we present very strong evidence for the detection of two 1993 seismic events with epilinear sources. We are aware of only one model that predicts seismic line events with frequency of one or two a year, namely the passage of "nuggets" of strange quark matter (SQM) through the earth.

In 1984, Witten [1] pointed out that, while matter made of up and down quarks is not stable, because ups and downs condense to form protons and neutrons, matter made of up, down, and strange quarks, SQM, may well be stable. This is because of the roughly 10% decrease in kinetic energy from having three Fermi seas with which to satisfy the Pauli principle instead of just two. Witten also suggested a scenario for early universe SQM nugget production, variations of which are still under debate [2], as well as the possibility of strange quark nuggets (SQN's) as dark matter candidates [3].

SQN's would not be limited in total baryon number [4] as is ordinary matter. Thus very large nuggets of SQM are possible. They would have nuclear densities ($\sim 10^{14}$ gm/cm$^3$). Because of the larger mass of the strange quark, an SQN with 3A quarks would have an excess of positively charged quarks over strange (negatively charged) quarks, and hence a net positive charge from "nuclear particles" which would be balanced by an electron cloud. For $M>10^{-9}$ gram, the cloud would be mostly inside the nuclear part of the SQN. The SQN would be nearly neutral and, with high mass and low abundance, would not interact with electromagnetic energy, hence it's suitability as a dark matter candidate. Finally, Witten [1] suggested looking for seismic signals from SQN's passing through the earth, an idea considered, among others, by deRujula and Glashow [5] in more detail.

This possibility motivated our work, but our detection of two epilinear source events could reflect other possible unknown phenomena. Two of us [ETH and VLT] examined detection of SQN seismic signals via a Monte Carlo calculation [6]. Briefly, a ton sized SQN would have dimensions of about 20 microns, the size of a blood cell. As it passed through the earth it would break inter and intra-molecular bonds, like a stone dropped in water, producing a seismic signal. The rate of seismic energy [E] production would be given by

$$dE/dt = f \alpha \rho V^3$$

where $\alpha$ is the SQN cross section, $\rho$ is the nominal earth density, V is the SQN speed (a few hundred km/sec, the galactical viral velocity [6]), and f is the fraction of SQN energy loss that results in seismic waves rather than heat. Underground nuclear explosions have f of about 0.01, chemical ones about 0.02. The small size of SQN, which enhances coherence and depresses random motion and yields a high ratio of surface area to energy generating volume, implies that f might be larger for the SQN case.

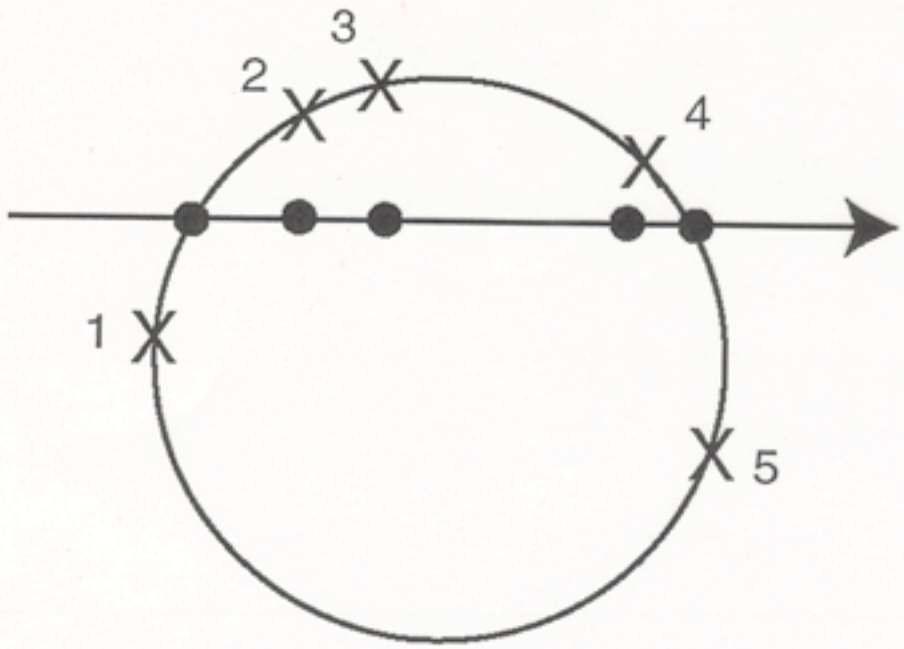


**Figure 1.** **Difference between point and line events. Xs represent seismic stations and dots are the corresponding points of closest approach.**

**An earthquake at the entry point would generate signals with the first arrival at station 1, then stations 2,3,4, and 5. A nuclearite passage would have the first arrival at station 4, near the exit, then stations 2, 1, 3, and 5.**

B. Travel Times

Seismic signal travel times through the earth are well known (IASPE1 [7]) and calibrated down to point source depths of 700 kilometers. For this study one of us (I. Tibuleac) generated additional travel times tables by ray tracing through the standard earth model [7] to a depth of 2880 kilometers: the core-mantle boundary. Signals that travel through the core are quite complex due to reflections and refractions at the boundaries, and hence were not considered in this study. The fact that the core is roughly half an earth radius implies that roughly 75% of random strikes will not enter the core.

The travel time tables generated were compared to published data [7] down to 700 kilometers and were calibrated with signals reflected from the core-mantle interface, and are in good agreement with both.

# Strangelet Search with AMS

Signal is low Z/A: not consistent with any normal nucleus

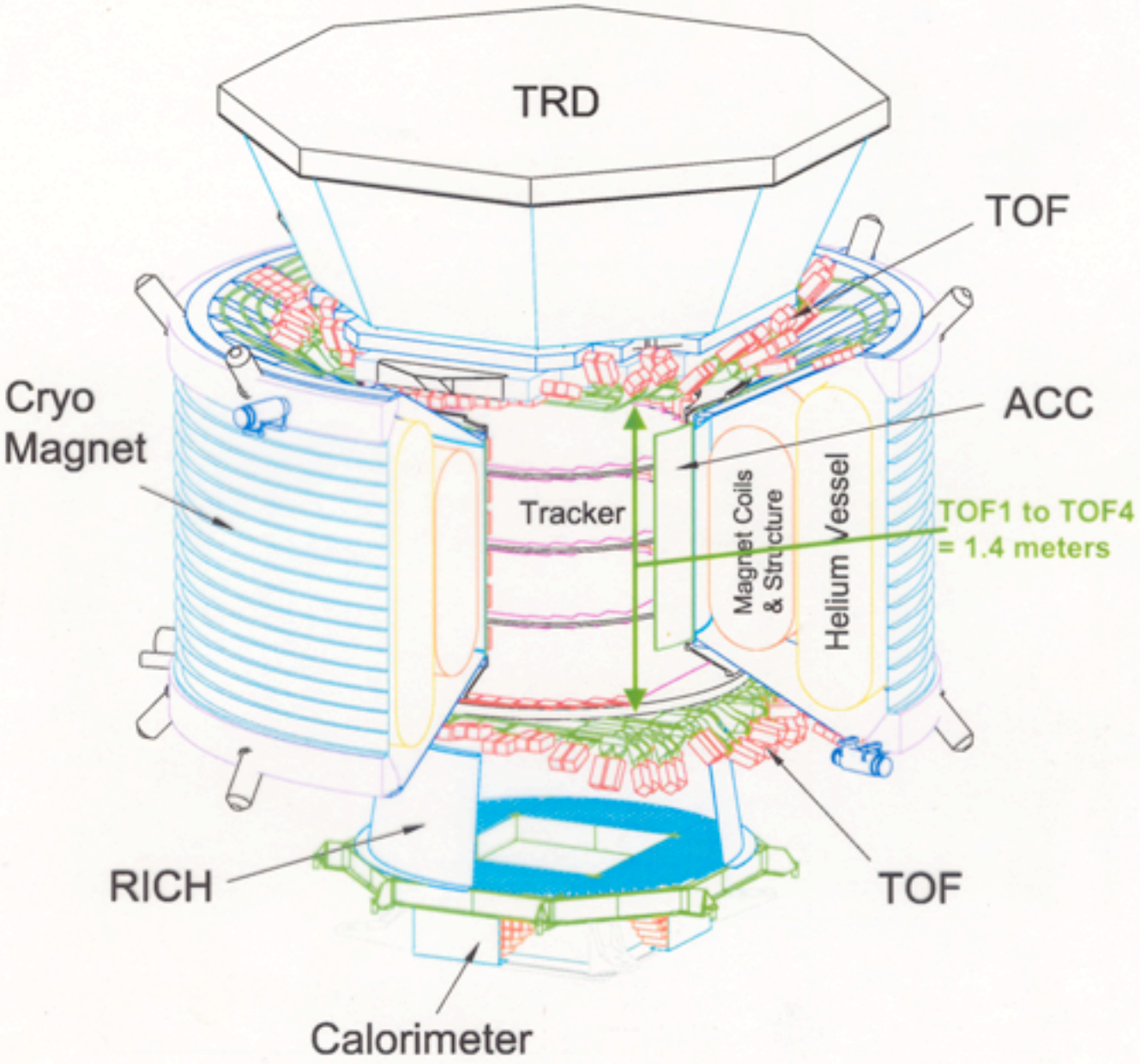


AMS can measure rigity, velocity, and charge (Z) over a certain region and thus can measure a mass and Z/A

Over a larger region, where the charge measurement is saturated, and/or the rigidity is above some maximum, one can still tell that a track is *not* a normal mucleus.

# Propagation of Strangelets in the Galaxy

- **Bound to Magnetic Field**
- **Undergo Interactions**
- **Accelerated in Super Nova Shock Waves**

**Expected to Behave Like Cosmic Ray Nuclei:**

$$dN(E)dE \propto E^{-2.5}$$

**Confinement time ~ $10^7$ y**

# Strangelet Flux at AMS
## (near Earth) J. Madsen

**Geomagnetic cutoff means only part of spectrum is visible near earth**

**Assume:** $dN(E)dE \propto E^{-2.5}$ (E = K.E./Baryon)

**Lowest velocity > 0.01c**
**(Supernova Shock wave)**

$R_{min} = 6$ GeV/c

CFL Relation: $Z=0.3\ A^{2/3}$

**Then:**

$$F = 5 \times 10^5\ m^{-2}\ y^{-1}\ sterad^{-1}$$

x Rate of Strange Star Collisions / $(10^{-4}/y)$

x Mass Ejected per Collision / $(0.01 M_{SUN})$

x Galactic Volume / $(100 kpc^3)$

x Confinement Time / $(10^7\ y)$

Estimate does not include absorption or loss of stglts on "way" to earth.

$$F = 5 \times 10^5 \text{ m}^{-2} \text{ y}^{-1} \text{ sterad}^{-1}$$

*This is a large flux!*

- AMS ~ 0.5 $m^2$ sterad
- Plenty of "wiggle room" for assumptions
- If nothing is seen in the 2-3 years that AMS will run there is little hope that stable SQM at zero pressure exists.

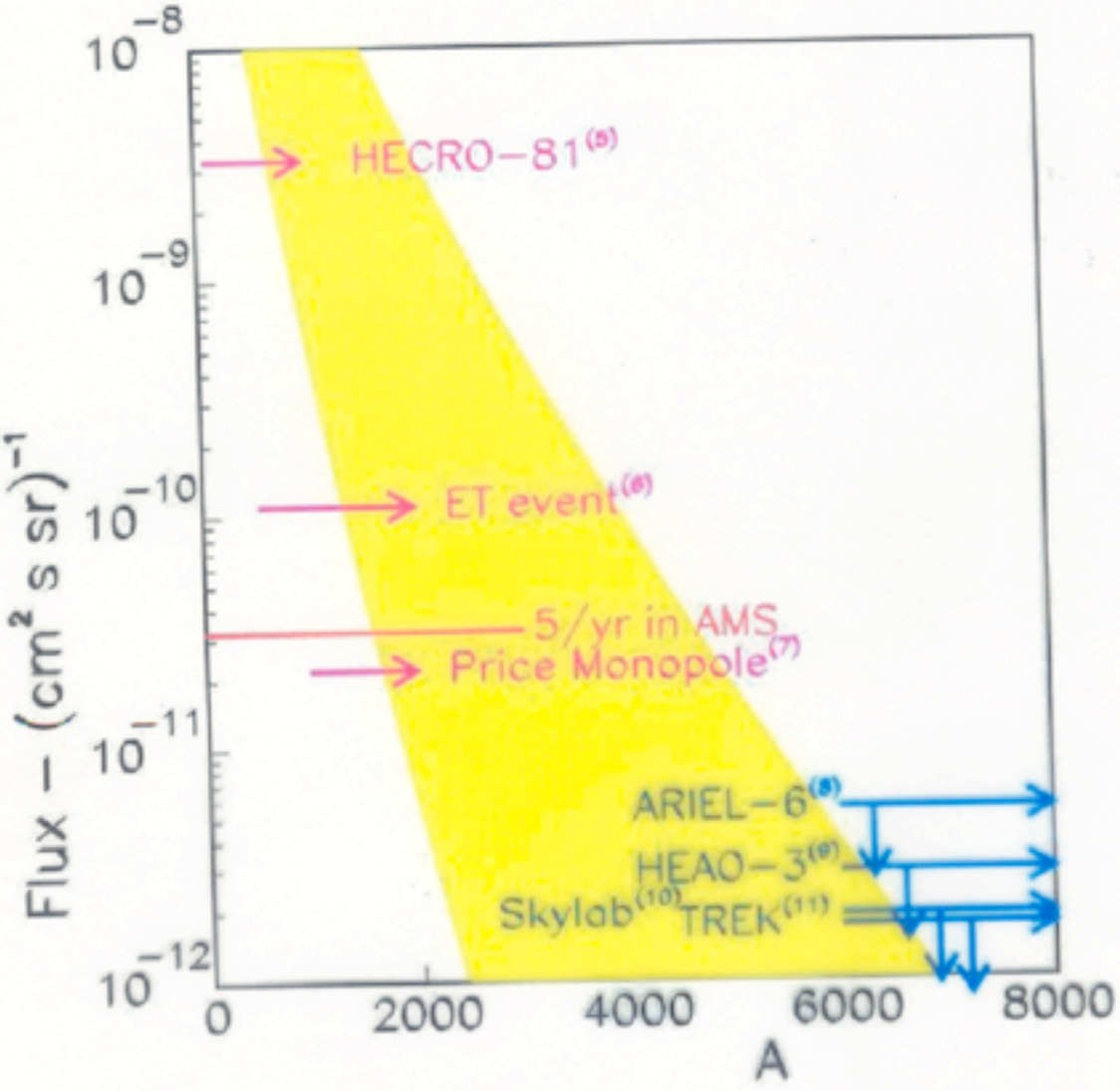
$10^{-8}$
$10^{-9}$
$10^{-10}$
$10^{-11}$
$10^{-12}$
Flux – $(cm^2\ s\ sr)^{-1}$
HECRO–81[5]
ET event[6]
5/yr in AMS
Price Monopole[7]
ARIEL–6[8]
HEAO–3[9]
Skylab[10]
TREK[11]
0
2000
4000
6000
8000
A

# Regions Accessible to AMS

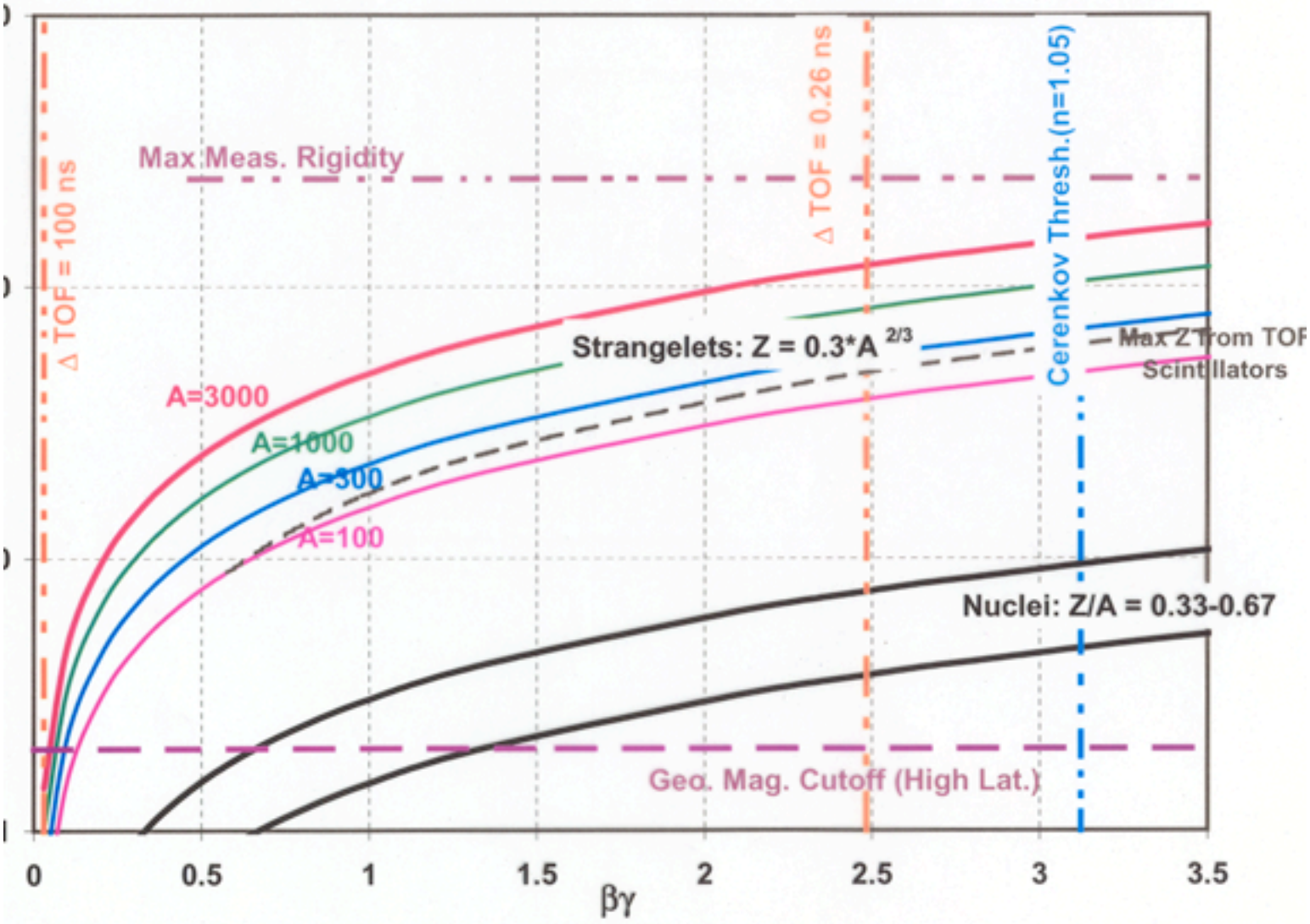

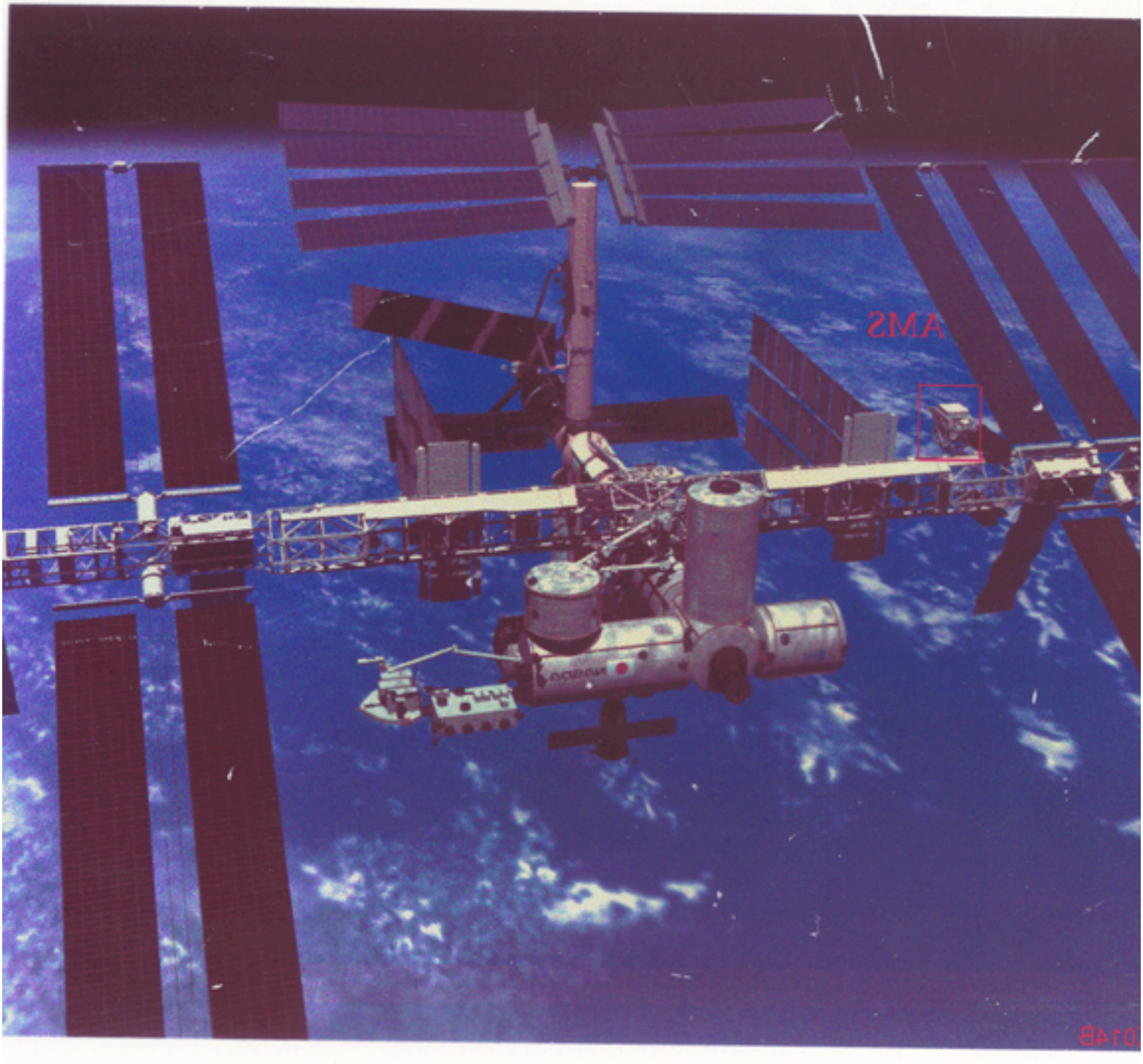
AMS

February 20, 2002

Laura Feiveson
Report

First I will use the upper and lower bounds of the absorbance coefficients to get a more accurate estimate of the number of strangelets hitting the surface.

The upper and the lower limits are: e^(-A^(2/3)*.04) and e^(-A^(2/3)*.08)

I need to multiply these numbers by the estimated densities that have already been calculated in the previous report. Then using the estimate that earth is silicon which has a density of 5*10^22 atoms per cubic centimeter and that water has a density of about 3.3*10^22 molecules per cubic centimeter, I will also find the lower and upper bounds of the number of strangelets per each atom of silicon (or molecule of water in the ocean).

The result:

**The density of strangelets in the earth's crust**

| | number/cm3 | | number/silicon atom | |
|---|---|---|---|---|
| Baryon Value | Lower Limit | Upper Limit | Lower | Upper |
| 50 | 1.99E+03 | 3.42E+03 | 3.98E-20 | 6.84E-20 |
| 100 | 4.10E+02 | 9.72E+02 | 8.22E-21 | 1.95E-20 |
| 1000 | 3.06E-02 | 1.67E+00 | 6.13E-25 | 3.35E-23 |
| 2000 | 1.03E-04 | 5.87E-02 | 2.05E-27 | 1.18E-24 |
| 3000 | 1.13E-06 | 4.63E-03 | 2.26E-29 | 9.27E-26 |
| 4000 | 2.20E-08 | 5.24E-04 | 4.40E-31 | 1.05E-26 |
| 5000 | 6.24E-10 | 7.49E-05 | 1.25E-32 | 1.50E-27 |

**The density of strangelets in the ocean**

| | number/cm3 | | number/molecule of water | |
|---|---|---|---|---|
| Baryon Value | Lower Limit | Upper Limit | Lower | Upper |
| 50 | 1.37E+07 | 2.36E+07 | 4.11E-16 | 7.07E-16 |
| 100 | 7.23E+06 | 1.71E+07 | 2.16E-16 | 5.12E-16 |
| 1000 | 1.35E+04 | 7.38E+05 | 4.04E-19 | 2.21E-17 |
| 2000 | 1.23E+02 | 7.04E+04 | 3.68E-21 | 2.11E-18 |
| 3000 | 2.39E+00 | 9.81E+03 | 7.15E-23 | 2.93E-19 |
| 4000 | 7.09E-02 | 1.69E+03 | 2.12E-24 | 5.05E-20 |
| 5000 | 2.79E-03 | 3.36E+02 | 8.35E-26 | 1.00E-20 |

# Number of Strangelets Expected on the Surface of the Moon

| Baryon Value | Stopping Line | Volume of Moon to Stopping Line |
|---|---|---|
| 50 | 138 | 5.01 E 19 |
| 100 | 52 | 1.89 E 19 |
| 1000 | 1.8 | 6.53 E 17 |
| 2000 | 0.63 | 2.29 E 17 |
| 3000 | 0.35 | 1.27 E 17 |
| 4000 | 0.23 | 8.35 E 16 |
| 5000 | 0.17 | 6.17 E 16 |
| | 7 | 6.17 E 16 |

**Use the biggest one from the table above: 136 cm**

√ Density in the top 138 cm (no./cc)

| Baryon Value | Lower | Upper |
|---|---|---|
| 50 | 3.68 E 14 | 6.35 E 1 |
| 100 | 9.75 E 13 | 2.31 E 14 |
| 1000 | 1.83 E 10 | 1.00 E 14 |
| 2000 | 8.34 E 07 | 4.77 E 12 |
| 3000 | 1.08 E 06 | 4.43 E 09 |
| 4000 | 2.40 E 04 | 5.73 E 08 |
| 5000 | 7.58 E 02 | 9.10 E 07 |

Density per silicon (no./atom)

| Lower | Upper |
|---|---|
| 7.39 E-09 | 1.27 E-08 |
| 1.95 E-09 | 4.62 E-09 |
| 3.67 E-13 | 2.00 E-11 |
| 1.67 E-15 | 9.56 E-13 |
| 2.16 E-17 | 8.88 E-14 |
| 4.81 E-19 | 1.15 E-14 |
| 1.52 E-20 | 1.82 E-15 |

**Seismic Search for Strange Quark Matter**

Vigdor Teplitz
Goddard Space Flight Center

Two decades ago, Witten suggested that the ground state of matter might be material of nuclear density made from up, down and strange quarks. Since then, much effort has gone into exploring astrophysical and other implications of this possibility. For example, neutron stars would almost certainly be strange quark stars; dark matter might be strange quark matter. Searches for stable strange quark matter have been made in various mass ranges, with negative, but not conclusive results. Recently, we [D. Anderson, E. Herrin, V. Teplitz, and I. Tibuleac, Bull. Seis. Soc. of Am. **93**, 2363 (2003)] reported a positive result for passage through the Earth of a multi-ton "nugget" of nuclear density in a search of about a million seismic reports, to the U.S. Geological Survey for the years 1990-93, not associated with known Earthquakes. I will present the evidence (timing of first signals to the 9 stations involved, first signal directions, and unique waveform characteristics) for our conclusion and discuss potential improvements that could be obtained from exploiting the seismologically quieter environments of the moon and Mars.

# Gravitational wave detection on the Moon and the moons of Mars

Ho Jung Paik and Krishna Yethadka Venkateswara
Department of Physics, University of Maryland, College Park, MD 20742, USA

**Abstract**. The Moon and the moons of Mars should be extremely quiet seismically and could therefore become sensitive gravitational wave detectors, if instrumented properly. Highly sensitive displacement sensors could be deployed on these planetary bodies to monitor the motion induced by gravitational waves. A superconducting displacement sensor with a 10-kg test mass cooled to 2 K will have an intrinsic instrument noise of $10^{-16}$ m $Hz^{-1/2}$. These sensors could be tuned to the lowest two quadrupole modes of the body or operated as a wideband detector below its fundamental mode. An interesting frequency range is 0.1 ~ 1 Hz, which will be missed by both the ground detectors on the Earth and LISA and would be the best window for searching for stochastic background gravitational waves. Phobos and Deimos have their lowest quadrupole modes at 0.2 ~ 0.3 Hz and could offer a sensitivity $h_{min} \leq 10^{-22}$ $Hz^{-1/2}$ within their resonance peaks, which is within two orders of magnitude from the goal of the Big Bang Observer (BBO). The lunar and Martian moon detectors would detect many interesting foreground sources in a new frequency window and could serve as a valuable precursor for BBO.

PACS numbers: 04.80.Nn, 95.55.Ym

## 1. Introduction

Due to lack of plate tectonics and its spin locked to its revolution, the Moon is very quiet seismically. Its total seismic energy release per year is estimated to be $10^9$ times lower than the Earth (Goins *et al* 1981). Moonquakes are driven mainly by tidal deformation due to the orbit eccentricity (0.05) and occur within a few days from the perigee (Lammlein *et al* 1974). With the absence of ocean waves and winds, the seismic noise level between moonquakes may be extremely low. Conditions should be similar on the moons of Mars. Of the two Martian moons, Deimos is especially interesting since it is farther out from Mars and its orbit eccentricity is only 0.003. This leads to an interesting possibility that the entire Moon and the moons of Mars could be instrumented as sensitive resonant-mass gravitational wave (GW) antennas.

This is exactly what Weber attempted to do in his ill-fated Apollo 17 Lunar Surface Gravimeter Experiment. His gravimeter was designed to monitor free oscillations of the Moon, possibly induced by GWs from astrophysical sources. In view of NASA's new initiative of Moon/Mars exploration, it is timely to revisit the idea of using planetary bodies as GW detectors.

## 2. Spherical antenna with superconducting displacement sensors

Although Phobos and Deimos are highly irregular in shape, the Moon is nearly spherical. A spherical antenna has the advantage of having a uniform cross section for all sky. Further, the amplitudes of its five degenerate quadrupole modes can be combined to determine the four unknowns: source direction ($\theta$, $\phi$) and wave polarization ($h_+$, $h_-$), and the remaining degree of freedom can be used to discriminate against non-GW disturbances (Wagoner and Paik 1977). Only quadrupole modes couple to spin-2 GWs. The TIGA (truncated icosahedral gravitational-wave antenna) configuration of six *radial* transducers (see Figure 1) has been shown to preserve the

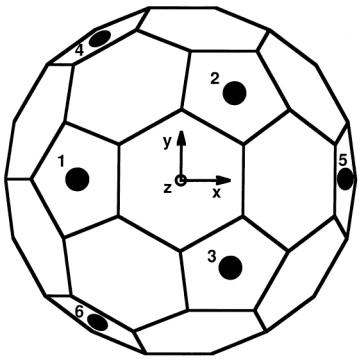


**Figure 1. TIGA configuration.**

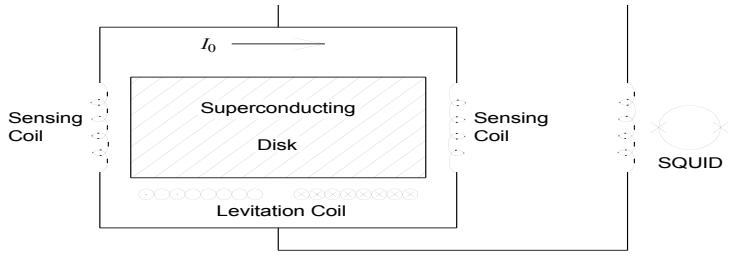


**Figure 2. Schematic of superconducting displacement sensor.**

five-fold degeneracy and omni-directionality (Johnson and Merkowitz 1993). We find that the same holds true for *tangential* transducers.

A highly sensitive tangential, or horizontal, displacement sensor could be constructed by combining a magnetically levitated test mass with a superconducting inductive transducer (Paik 1976). Figure 2 shows a schematic of the superconducting displacement sensor. The horizontal displacement of the levitated superconducting disk modulates the magnetic flux produced in each sensing coil, inducing a flux in the SQUID input coil proportional to the displacement.

The power spectral density of its intrinsic instrument noise can be shown to be

$$S_x(f) = \frac{4}{m\omega^4}\left\{k_B T\frac{\omega_0}{Q_0} + E_A(f)\frac{1}{2\beta\eta\omega_0^2}\left[(\omega_0^2-\omega^2)^2 + \left(\frac{\omega_0\omega}{Q_0}\right)^2\right]\right\}, \qquad (1)$$

where $m$, $f_0 = \omega_0/2\pi$, and $Q_0$ are the mass, resonance frequency, and quality factor of the test mass; $\beta$, $\eta$, and $E_A(f)$ are the transducer energy coupling constant, amplifier coupling efficiency, and SQUID energy resolution; and $f = \omega/2\pi$ is the signal frequency, respectively. With somewhat optimistic but feasible values of $m = 10$ kg, $f_0 = 0.3$ Hz, $T = 2$ K, $Q_0 = 10^8$, $2\eta\beta = 0.5$, $E_A(f) = 10^{-31}$ J Hz$^{-1}$, we find $S_x^{1/2}(f) \approx 10^{-16}$ m Hz$^{-1/2}$ at $f = 0.3$ Hz. This displacement sensor would be $10^6$ times more sensitive than the Apollo lunar seismometers (Lammlein *et al* 1974).

## 3. Two modes of detector operation

There are two ways of operating a planetary gravitational wave detector: (1) as a *wideband* detector below its lowest mode, where the planetary body acts as a rigid platform, and (2) as a *resonant* detector, by tuning the displacement sensors to the fundamental ($n = 1$) or second harmonic ($n = 2$) quadrupole mode ($\ell = 2$), which couple strongly with GWs (Lobo 1995).

To obtain approximate sensitivities of the spherical detector in the two modes of operation, the detector response is approximated as that of a cylinder and the GW power spectral density is summed over the six displacement sensors with appropriate geometric factors. The detector response can be written as

$$(\ddot{x} - \ddot{\xi}) + \tau_0^{-1}(\dot{x} - \dot{\xi}) + \omega_0^2(x - \xi) = \frac{1}{2}\ddot{h}R - \ddot{\xi}, \qquad (2)$$

where $x$ and $\xi$ are the displacement of the test mass and the planet's surface, respectively, and $R$ is the radius of the planet.

Below its fundamental frequency ($f < f_1$), a planetary body will act as a rigid platform, which does not respond to GWs or the moonquakes: $\xi = \dot{\xi} = \ddot{\xi} = 0$. To maximize the sensitivity of the wideband detector, the test masses must be almost free ($f_0 < f$). The GW power spectral density summed over six sensors then becomes

$$S_h(f) \approx 10\left(\frac{2}{R}\right)^2 S_x(f). \tag{3}$$

It is interesting to compare the potential sensitivity of a wideband spherical detector with that of LISA. The Moon has $f_1 \approx 10^{-3}$ Hz. If the displacement sensors are tuned to $f_0 = 10^{-4}$ Hz, the sensor-noise-limited detector sensitivity becomes $S_h^{1/2}(f) \approx (10^{-4}\ \text{Hz}/f)^2 3\times10^{-18}\ \text{Hz}^{-1/2}$ for $f = 10^{-4} \sim 10^{-3}$ Hz. This is comparable to the sensitivity of LISA. Deimos, which is 270 times smaller in diameter than the Moon, will permit a wideband operation below $f_1 \approx 0.3$ Hz. The sensitivity is again found to be comparable with LISA in the frequency band $f = 0.1 \sim 0.3$ Hz.

Above the fundamental frequency ($f > f_1$), the driving terms in Eq. (2) cancel except at the quadrupole mode frequencies $\omega_n$ (Chen and Thorne 2004), where we obtain

$$x - \xi = -0.2i\omega_1^2 hR \frac{\omega^2}{\omega_n^2 - \omega^2 + i\omega\omega_n/Q_n} \frac{\omega^2}{\omega_0^2 - \omega^2 + i\omega\omega_0/Q_0}. \tag{4}$$

The GW power spectral density summed over six sensors becomes

$$S_h(f) \approx \frac{10}{(0.2\omega_1^2 R)^2}\left[(\omega_n^2 - \omega^2)^2 + \left(\frac{\omega\omega_n}{Q_n}\right)^2\right] S_x(f). \tag{5}$$

With $Q_1 \approx 2000$, as measured on the Moon, this leads to the sensor-noise-limited sensitivities for the Moon and Deimos: $S_h^{1/2}(f) \approx 2\times10^{-21}\ \text{Hz}^{-1/2}$ at $f = f_1 = 10^{-3}$ Hz and $S_h^{1/2}(f) \approx 3\times10^{-20}\ \text{Hz}^{-1/2}$ at $f = f_1 = 0.3$ Hz, respectively.

Figure 3 compares the sensitivities of the Moon and Deimos with those of LIGO, LISA, and BBO (Big Bang Observer). Also shown in the figure are expected signals from foreground blackhole, neutron star, and white dwarf binaries, as well as the stochastic background from the Big Bang. Deimos looks especially attractive because it will open a new frequency window between the ground detectors and LISA, and its sensitivity comes within two orders of magnitude from the goal of BBO, albeit within a very narrow bandwidth (Phinney 2004). Such a detector will detect many interesting foreground sources and will serve as a valuable precursor to BBO.

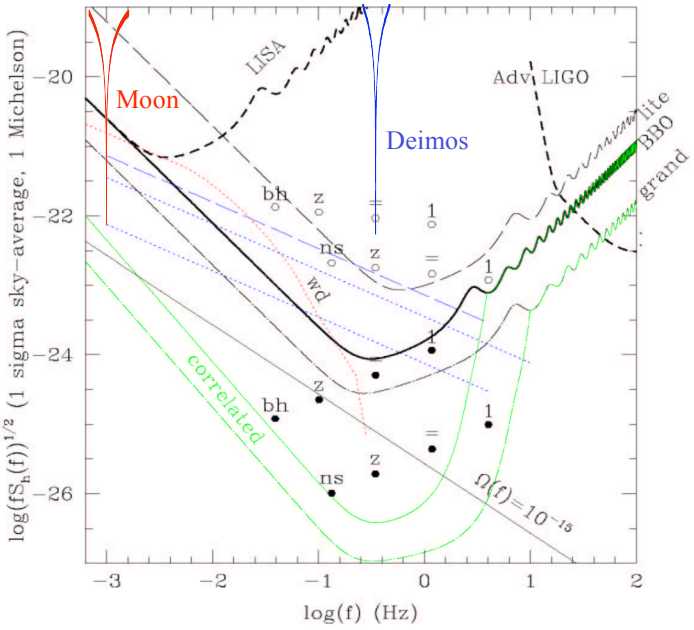


**Figure 3. Sensitivities of the Moon and Deimos compared with LIGO, LISA and BBO.**

## 4. Technology requirement

A critical technology that needs to be developed to enable GW detection on the Moon or a Martian moon is a space-qualified "vibration-free" cryocooler for $T \leq 4$ K. Several types of closed-cycle refrigerators are under development for applications in infrared astronomy missions. The pulse-tube cryocooler operates at 55 K and is almost free of vibration (Ross *et al* 1998). An additional cooling stage could be added to this cooler to reach 4 K and below. Another option of achieving vibration-free refrigeration is the reverse-Brayton cryocooler. The crycoolers are power-hungry. So it appears that RTGs (Radioisotope Thermal Generators) will be required to provide power continuously through the day-night cycle.

To obtain the projected sensitivity, the superconducting displacement sensor needs to be improved in two fronts. The high quality factor ($Q \approx 10^8$) must be demonstrated in a magnetically levitated superconducting test mass. For low-frequency operation ($f < 0.1$ Hz), it is desirable to upconvert the signal frequency to above the 1/f corner frequency of the SQUID. An ac bridge transducer is under development to achieve this goal (Chui *et al* 2004).

In addition to the cryocooler vibration, there are numerous other sources of seismic noise: moonquakes, thermal quakes at sunrise (> 1 Hz, diurnal), meteorite impacts, and human activities. The seismic noise is the most likely limiting error source, especially for experiments on the Moon. It is therefore important to develop a procedure to veto the seismic excitation by using the unique tensor nature of GW. It is highly desirable to survey the seismic background of the moons with superconducting displacement sensors prior to a GW experiment.

Gravity noise will arise from tidal deformation and thermal expansion of the ground and the apparatus. However, these are not of concern since they will occur at extremely low frequencies, well outside the signal bandwidth. The instrument could be buried in the regolith to reduce its temperature variation. The levitated test masses will be electrically charged by cosmic rays. This will also occur at very low frequencies outside the signal bandwidth.

## Acknowledgment

We have benefited from discussions with Kip Thorne, Yanbei Chen, Sterl Phinney, Yosio Nakamura, Don Strayer, and Vol Moody. This work was supported by a NASA grant under NRA-01-OBOR-08-E and by JPL through its appointment of one of us (HJP) as a Distinguished Visiting Scientist.

## References

Chen Y and Thorne K S 2004 Private communication
Chui T *et al* 2004 *35th COSPAR Scientific Assembly*, Paris, France
Goins N R, Dainty A M and Toksöz M N 1981 *J. Geophys. Res*. **86** 378
Johnson W W and Merkowitz S M 1993 *Phys. Rev. Lett*. **70** 2367
Lammlein D R *et al* 1974 *Rev. Geophys. Space Phys*. **12** 1
Lobo J A 1995 *Phys. Rev. D* **52** 591
Paik H J 1976 *J. Appl. Phys*. **47** 1168
Phinney S 2004 Private communication
Ross R G 1998 *Proceedings of the 10th International Cryocooler Conference, Monterey, California*
Wagoner R V and Paik H J 1977 *Experimental Gravitation* (Rome: Accademia Nazionale dei Lincei) p 257

**Self Organized Critical Phenomena Near the Superfluid Transition**

Robert Duncan
University of New Mexico

New phenomena have been observed on the self-organized heat transport state near the superfluid transition in helium-4, including a new temperature / entropy wave that travels only against the heat flux direction, and superfluid dissipation that is a factor of about ten times larger than conventional measurements when taken immediately prior to the formation of this self-organized state. While extensive theoretical and experimental studies have been conducted, the underlying microscopic method that permits this fascinating state to form has yet to be confirmed experimentally. These self-organized heat transport measurements may be repeated robotically on the surface of the Moon or Mars in a relatively simple measurement apparatus. Such measurements would provide a different gravitational field from that on the Earth, resulting in a different self-organization. This may help determine the underlying microscopic process that permits this self-organized state to form. Other measurements of dynamical effects near the superfluid transition, similar to those planned originally as part of the DYNAMX, CQ, and CP experiments, may be performed as the spacecraft is weightless during the time it is in route to its destination.

**Lunar Helium 3 - Preliminary Prospectus**

D. M. Lee and J. D. Reppy
Cornell University

Introduction and Executive Summary

It has been known since the Moon landings that $^3$He was present in the top layer of the lunar surface (the regolith). Estimates of $10^6$ tons of $^3$He contained in the lunar regolith have been made on the basis of the gases evolved from lunar rocks that have been returned to the Earth. Helium is a major component of the solar wind. The gases trapped and stored in the regolith are mainly hydrogen (96%) and helium (4%). The helium gas in rocks recovered from the Sea of Tranquility contains 1 part in 2600 $^3$He. These gases can be recovered from lunar soils and rocks by heating to about 600ºC.

We are interested in pursuing further studies of the gas content of rocks returned from the lunar regolith by our astronauts. The purpose of these studies will be to increase our knowledge of the availability of $^3$He on the Moon and to develop the best procedures to extract $^3$He gas samples and to store them in the liquid state to facilitate their transfer back to the Earth. For this purpose, it would be desirable if lunar samples from the regolith could be furnished by NASA for these studies. The kinds of questions we would like to answer are as follows:

1. What is the best temperature for extracting the gas? Should the samples be crushed?
2. How well do the volatile solar wind gases ($H_2$, $^4$He and $^3$He) diffuse through the lunar material for various temperatures?
3. What are the best methods for collecting the gases?
4. What are the best ways to determine the relative concentrations of $H_2$, $^4$He and $^3$He?
5. What are the best ways to separate and purify the $^3$He?
6. What are the best ways to store the gases in the lunar environment? What cryogenic facilities will be needed on the lunar surface?

It should be relatively straightforward to set up laboratory experiments to answer questions 1 – 5 if kilogram quantities of lunar regolith materials could be made available for study.

$^3$He is present on the Moon's surface in amounts typically between 10 and 30 parts per billion. Taking the smaller figure (1 part in $10^8$), we would have $10^{-8}$ kg or $10^{-5}$ grams in each kg of lunar material ($3.3 \times 10^{-6}$ moles). If we take the molar volume of liquid $^3$He to be ~ 30 cm$^3$, roughly 1 mm$^3$ of liquid $^3$He can be extracted from 1 kg of lunar rock.

Questions 1 and 2 can be answered in relatively straightforward high-temperature experiments by studying the time required for gases to evolve from the lunar samples. Mass spectrometric methods can be used to determine the gas content.

The best method for dealing with question 3 is to employ cryopumping to collect the $H_2$, $^3$He, and $^4$He in liquid form. The relative concentrations can be determined by mass spectroscopy or, for the case of $^3$He and $H_2$, by performing nuclear magnetic resonance experiments on the liquids. Cryogenic separation of the gases (question 5) can be accomplished via selective distillation or via superleak methods. Question 6 almost certainly requires a cryogenic solution and involves cryocoolers to be set up on the Moon's surface.

More details are provided in the discussion to follow.

Objectives and their value

$^3$He is extremely rare on Earth. It is produced artificially in nuclear reactors when neutrons in the reactor core collide with lithium nuclei. The tritium produced in the ensuing nuclear reactions decays to $^3$He with a half-life of about 12.5 years. Much of the tritium produced is employed as a component of thermonuclear weapons. As time goes by, the tritium must be replenished and the $^3$He resulting from tritium decay is saved.

$^3$He from the solar wind can also be found in the Earth's atmosphere in very minute quantities. Because the $^3$He is very light, it tends to escape from the Earth's atmosphere, so that the steady state concentration of $^3$He corresponds to a balance between the solar wind input and the loss via escape into space.

In the case of the Moon, there is virtually no atmosphere, so the solar wind directly impacts the surface as it has done for several billion years. Therefore, gases such as hydrogen and helium can become trapped and stored in the rocks and soils of the lunar regolith (the top few meters of the lunar surface). The purpose of the planned program is to study the lunar soils and rocks to determine the concentration of $^3$He gas in the lunar regolith and to determine the feasibility of extracting the $^3$He and returning it to Earth. Previous studies of lunar samples obtained by our astronauts have revealed relatively large concentrations of $^3$He. In fact, by some estimates there are a million tons of $^3$He in the surface regolith of the Moon. We believe that sophisticated robotics and sophisticated cryogenics will ultimately be required to carry out any large-scale mission to collect and return large samples of $^3$He. Participation by astronauts may be required for some phases of such a project.

There are two major applications for $^3$He being considered. The first is the use of nuclear spin-polarized $^3$He gas in magnetic resonance imaging of the interior of the lungs. Testing of this technique has been successful and large-scale clinical applications should be possible if $^3$He gas becomes readily available. The second application is still many years away - the use of $^3$He in nuclear fusion reactors employing deuterium–$^3$He and $^3$He–$^3$He reactions. Although considerable progress in fusion research has been made, a working fusion reactor is not yet operational. The present emphasis is on inertial confinement (laser fusion) and magnetic confinement (tokomak). The initial stages involve the deuterium–tritium (D-T) reaction that has by far the lowest ignition temperature. The main disadvantage of the D-T reaction is that most of the energy is emitted in the form of fast neutrons. This energy must be converted into heat just as in a conventional fission reactor. Furthermore, the neutrons can react with the containment vessel walls to produce dangerous radionuclides. In the D-$^3$He and the $^3$He – $^3$He reactions, a large fraction of the energy is in the form of the kinetic energy of fast charged particles that can be used to directly generate electricity. Fusion reactors utilizing $^3$He are being developed by the fusion group (Gerald Kulcinski) at the University of Wisconsin.

There are other possible applications. For example, owing to the large reaction cross section for neutron-$^3$He reactions, $^3$He can be used in neutron detectors and in neutron shielding. Finally, $^3$He is highly valued as an essential cryogenic fluid that is extremely useful for research at temperatures below 0.5 K ranging down to below 1 mK.

How to do it

In the early twentieth century, a major source of $^4$He gas was the monazite sand deposits in India. In fact, the first helium liquefier built by Heike Kammerling-Onnes in the first decade utilized helium extracted from monazite sands by heating the sand to 1000ºC. It has been shown that lunar rocks contain various gases that can be extracted via heating to 600ºC. The main lunar gaseous components are hydrogen (96%) and helium (4%), with trace amounts of other gases. Previous samples have shown that the lunar helium contains 1 part in 2600 $^3$He, so the gases that evolve from the heating process should contain about 15 parts per million of $^3$He.

We envision an overall program that would involve three basic steps as follows:

(1.) Extraction and Collection
(2.) Purification and
(3.) Transport back to Earth.

A large-scale program would require a major commitment by NASA. University laboratories such as Cornell, and the Jet Propulsion Laboratory, should be involved to provide the research necessary to plan such a program. These laboratories have employed $^3$He in their experiments for several decades, and the experience they possess with the required cryogenic techniques gives them insights into the problems and solutions that will arise from the harvesting processes. Focused engineering will be necessary to design and construct large-scale, reliable systems to achieve ultimate success. Much of the exploration and processing will require the use of sophisticated robotics. The JPL-Cornell group has made great strides in this direction with the highly successful operation of the Mars landers Spirit and Opportunity, in spite of a several-minute delay for radio signals to propagate between the Earth and Mars. The much shorter time delay for signals to reach the Moon (< 2 Sec.) allows essentially real-time processing and control. Furthermore, manned missions can be utilized to service and monitor the equipment on the lunar surface.

(a.) Extraction

Mining the Moon presents a formidable challenge that will most likely take many years to bring to fruition, but which will no doubt provide technological spin-offs for Earth-bound applications. Since $^3$He is thought to be quite widely distributed on the lunar surface, the mining and extraction equipment must be mobile, so that as one area is mined out, the equipment can move on to more virgin areas. Techniques for mining will involve heating the lunar rock and soil to 600ºC and then collecting the volatile gases associated with solar wind deposition. It is not clear whether or not the rock and soil must first be crushed to assure optimum yield.

Collecting the gases may require cryopumping for best efficiency. Possibly, precompression by turbopumps of the gases thermally evolved from the rock samples could reduce the size of pumping tubes into the cryogenic region for fast collection of the gas, further reducing the thermal load, already reduced by the low-temperature (as low as 40 Kelvins in some locations) environment. Cooling of the cryopumps could be accomplished by pulse-tube cryocoolers such as those manufactured by Cryomech with no low temperature moving parts, and having service intervals of 20,000 hours (3 years) only for exchange of filters in the circulating helium lines. (Currently these cryocoolers can handle loads of up to 1.5 watts).

Whereas some aspects of the automated mining procedure may seem daunting, the presence of solar power for the extraction of helium (especially for the heating of the rocks) is a plus. The presence of a good vacuum at the lunar surface simplifies preloading of ore into the helium extraction chamber, and could possibly allow for dramatically lighter-weight walls for the separation chamber, the cryopumping, and the cryogenic storage of the liquefied $^3$He than would be possible to use on Earth, where such structures need to support an atmospheric pressure difference. The good vacuum obviously helps with the problem of thermal insulation, as well.

(b.) Purification

The hydrogen (96%) and helium (4%) are the predominant volatile gases associated with solar wind deposition on the lunar surface. Samples sent back from the Sea of Tranquility contain a fraction of one part $^3$He to 2600 parts of $^4$He, so only a small amount of $^3$He must be separated from the large amounts of $^4$He and hydrogen. Schemes for such separation must be developed that also collect the valuable hydrogen and $^4$He. Distillation procedures must be worked out.

The pressure-temperature (PT) diagram for $H_2$, $^4$He and $^3$He are quite different, with $^3$He being the most volatile and $H_2$ being the least volatile. Other methods of separation to be considered are diffusion of hydrogen through a hot Pd leak or diffusion of helium through thin plastic membranes. Separation of $^3$He from $^4$He can also be accomplished with the help of superleaks.

Some of these processes will need liquid helium, so reliable helium liquefiers and possibly hydrogen liquefiers must be developed. The liquefiers may be based on the design of the above-described cryocoolers that, as mentioned, have no moving parts at low temperatures, thus improving their reliability. Also, helium and hydrogen must be stored in liquid form, so that lightweight containers (dewars) can be utilized. Storage as liquid would also facilitate (by reducing volume and mass) the return to the Earth. We note here that any mechanical refrigerators should be emplaced to maximize thermodynamic efficiency, whenever possible, by taking advantage of the large temperature gradients existing on the Moon. The temperatures at the equatorial region vary from 100K (-173 C) to 400 K (127 C) from predawn to high noon. During the sunlit period, solar concentrators can supply the heating to evolve the gases, which are then held in large bladders. During the cold night, the cooling operations will be performed with considerable advantage in the cold environment, so the power requirements can be much reduced. Thus, the extraction processes will be timed to coincide with the lunar monthly cycle of light and darkness.

(c.) Transport

As mentioned above, light-weight dewars can be designed and constructed for use in these operations. Such dewars would utilize the excellent vacuum ($\sim 10^{-13}$ torr) at the lunar surface for insulation, and would also employ layers of lightweight superinsulation to block heating by radiation. Liquid $^3$He will be stored in an interior cylindrical tank and would be surrounded by an annular tank containing the abundant liquid $^4$He to provide thermal shielding. The vacuum of space could provide pumping on the liquid $^4$He vapor to maintain the temperature of the $^3$He below its liquefaction temperature ($\sim$3 K). Valves must be provided to isolate the

external environment from the dewar vacuum and pump-out tubes during re-entry into the Earth's atmosphere.

Since helium is very light, relatively little energy would be required to attain lunar orbit. The lunar escape velocity is 2.4 km/s. Liquid hydrogen-liquid oxygen fuel, also extracted from the regolith minerals, would give 5km/s and rail guns (solar power) could give 4 km/s final velocities (well above escape velocity).

Clearly much work is necessary to refine concepts and to develop all the systems required. Since thermonuclear reactors are still in the early stages of research and development, adequate time remains to work out most of the problems associated with mining and returning large quantities of $^{3}$He back to the Earth for use in fusion power reactors. Application to lung diagnosis procedures will proceed as the $^{3}$He gas becomes more readily available.

## Getting started

This section presents a basic outline to initiate a study and research program.

(a.) Literature Search

The first thing to do is to make a thorough search through NASA files and the open literature to determine in more detail what is known about $^{3}$He on the lunar surface. The support by the NASA laboratories and the NASA repositories responsible for storage of materials recovered from the lunar surface will be needed.

(b.) Study Lunar Rock Samples

Further laboratory studies of lunar rock samples are definitely in order, since it is necessary to devise strategies for extraction of the volatile solar wind gases helium and hydrogen. The concentration of the various gases in the lunar rocks and soils must be determined. It is hoped that we can obtain lunar rock samples from NASA. The kinds of questions that need to be answered by these experiments are the following:

(i.) Do the rock samples need to be crushed?
(ii.) What is the optimum temperature for the most efficient extraction process?

In order to research (ii.), it might be useful to measure the diffusion rate of the various gases through the lunar rock and soil samples as a function of temperature. It is equally important to understand the mechanism by which the gases are held in the lunar regolith for billions of years. Why are these gases (especially non-reactive helium) trapped and stored so efficiently in the surface layers of the Moon? The optimum extraction temperature is related to the nature of this storage process and to the diffusion rates of the gases out of the rocks.

(iii.) Why are certain locations (especially those with concentrated iron titanium oxide) better at storing the gases?

Hopefully, controlled laboratory experiments can be devised to explain the retention and storage in the more optimum locations. Simulating the solar wind impinging on the lunar surface is expected to be very challenging, however, and would not be an immediate priority. More thought needs to go into this aspect of the study.

(c.) Collection and Characterization of Gas Samples

Heating lunar rocks and soils in a good vacuum will result in the evolution of trapped gases. $^4$He concentrations up to 70 parts per million are found in the regolith derived from titanium-rich basalts. One part in 2600 of this helium is $^3$He. Concentrations of $^3$He and $^4$He in these ranges are easily detected by mass spectrometers such as those that have been employed in our labs as helium leak detectors for many years. Some of this analysis has been done, but further lunar rock samples, if available, should be investigated for $^3$He and $^4$He content.

The second step in the initial study of lunar helium should be the collection of small bulk samples of helium obtained from the rock. Selective cold-trapping and cryopumping should help to select out the large concentrations of $H_2$, leaving samples composed mainly of $^3$He and $^4$He. These bulk gas samples can be condensed into a cell cooled to well below the normal (1-atmosphere) boiling temperatures of $^4$He and $^3$He (4.2 K and 3.2 K, respectively). Small samples of the bulk dilute helium mixture can be cooled to 4 mK in a dilution refrigerator and analyzed by nuclear magnetic resonance (NMR) at 270 Mhz in 9-Tesla magnetic fields. For these conditions, very large NMR signals have been seen at Cornell in samples containing a few hundred parts per million $^3$He, so for high enough fields and low enough temperatures, this method should provide a good analytical tool for developing processing techniques.

To further purify the dilute $^3$He-$^4$He mixtures, a superleak method can be used that relies on the properties of superfluid $^4$He. A superleak consists of a porous material with very small pores—typically finely ground jeweler's rouge or porous vycor glass can be used. The superfluid $^4$He will flow freely through a superleak, while the small $^3$He component is left behind. In other words, the $^3$He is filtered out. $^3$He can also be purified by distillation methods. At Cornell we have had experience with both types of purification apparatus.

A small-scale pilot study is envisioned which can be scaled up and adapted to lunar conditions. In this study, various schemes for extracting, collecting and concentrating $^3$He from lunar rocks and soils will be examined.

**Preparation for Space: Torsion Balance Fundamental Physics Experiments**

Jens Grundlach
University of Washington

We are developing ultra-sensitive torsion balances to perform tests of fundamental physics. Our ground-based investigations are either directly relevant to space-based experiments or are designed to test fundamental physics that could ultimately be tested with much higher precision using the environment of space. In particular we have built a continuously rotating torsion balance apparatus to test the equivalence principle with unprecedented sensitivity. Our measurements share numerous experimental details with proposed equivalence principle tests using satellites (e.g. STEP). With another experiment we are augmenting the strong equivalence principle test that uses lunar laser-ranging to the mirrors installed on the moon by the Apollo program.

# Experimental Design for the LATOR Mission

Slava G. Turyshev,*[a] Michael Shao,†[a] and Kenneth Nordtvedt, Jr.‡[b]

[a] *Jet Propulsion Laboratory, California Institute of Technology, Pasadena, CA 91109*
[b] *Northwest Analysis, 118 Sourdough Ridge Road, Bozeman MT 59715 USA*

This paper discusses experimental design for the Laser Astrometric Test Of Relativity (LATOR) mission. LATOR is designed to reach unprecedented accuracy of 1 part in $10^8$ in measuring the curvature of the solar gravitational field as given by the value of the key Eddington post-Newtonian parameter $\gamma$. This mission will demonstrate the accuracy needed to measure effects of the next post-Newtonian order ($\propto G^2$) of light deflection resulting from gravity's intrinsic non-linearity. LATOR will provide the first precise measurement of the solar quadrupole moment parameter, $J_2$, and will improve determination of a variety of relativistic effects including Lense-Thirring precession. The mission will benefit from the recent progress in the optical communication technologies – the immediate and natural step above the standard radio-metric techniques. The key element of LATOR is a geometric redundancy provided by the laser ranging and long-baseline optical interferometry. We discuss the mission and optical designs, as well as the expected performance of this proposed mission. LATOR will lead to very robust advances in the tests of Fundamental physics: this mission could discover a violation or extension of general relativity, or reveal the presence of an additional long range interaction in the physical law. There are no analogs to the LATOR experiment; it is unique and is a natural culmination of solar system gravity experiments.

PACS numbers: 04.80.-y, 95.10.Eg, 95.55.Pe

## I. INTRODUCTION

After almost ninety years since general relativity was born, Einstein's theory has survived every test. Such a longevity, along with the absence of any adjustable parameters, does not mean that this theory is absolutely correct, but it serves to motivate more accurate tests to determine the level of accuracy at which it is violated. Einstein's general theory of relativity (GR) began with its empirical success in 1915 by explaining the anomalous perihelion precession of Mercury's orbit, using no adjustable theoretical parameters. Shortly thereafter, Eddington's 1919 observations of star lines-of-sight during a solar eclipse confirmed the doubling of the deflection angles predicted by GR as compared to Newtonian-like and Equivalence Principle arguments. This conformation made the general theory of relativity an instant success.

From these beginnings, the general theory of relativity has been verified at ever higher accuracy. Thus, microwave ranging to the Viking Lander on Mars yielded accuracy $\sim$0.2% in the tests of GR [1–3]. Spacecraft and planetary radar observations reached an accuracy of $\sim$0.15% [4]. The astrometric observations of quasars on the solar background performed with Very-Long Baseline Interferometry (VLBI) improved the accuracy of the tests of gravity to $\sim$0.045% [5–7]. Lunar laser ranging, a continuing legacy of the Apollo program, provided $\sim$0.011% verification of GR via precision measurements of the lunar orbit [8–14]. Finally, the recent experiments with the Cassini spacecraft improved the accuracy of the tests to $\sim$0.0023% [15]. As a result general relativity became the standard theory of gravity when astrometry and spacecraft navigation are concerned.

However, the tensor-scalar theories of gravity, where the usual general relativity tensor field coexists with one or several long-range scalar fields, are believed to be the most promising extension of the theoretical foundation of modern gravitational theory. The superstring, many-dimensional Kaluza-Klein, and inflationary cosmology theories have revived interest in the so-called 'dilaton fields', i.e. neutral scalar fields whose background values determine the strength of the coupling constants in the effective four-dimensional theory. The importance of such theories is that they provide a possible route to the quantization of gravity and unification of physical law.

Recent theoretical findings suggest that the present agreement between Einstein's theory and experiment might be naturally compatible with the existence of a scalar contribution to gravity. In particular, Damour and Nordtvedt [16] (see also [17] for non-metric versions of this mechanism and [18] for the recent summary of a dilaton-runaway scenario) have found that a scalar-tensor theory of gravity may contain a 'built-in' cosmological attractor mechanism towards GR. A possible scenario for cosmological evolution of the scalar field was given in [11, 16]. Their speculation assumes that the parameter $\frac{1}{2}(1-\gamma)$ was of order of 1 in the early universe, at the time of inflation, and has evolved to be close to, but not

*Electronic address: turyshev@jpl.nasa.gov
†Electronic address: mshao@huey.jpl.nasa.gov
‡Electronic address: kennordtvedt@imt.net

exactly equal to, zero at the present time. In fact, the analyzes discussed above not only motivate new searches for very small deviations of relativistic gravity in the solar system, they also predict that such deviations are currently present in the range from $10^{-5}$ to $\sim 5 \times 10^{-8}$ of the post-Newtonian effects. This would require measurement of the effects of the next post-Newtonian order ($\propto G^2$) of light deflection resulting from gravity's intrinsic non-linearity. An ability to measure the first order light deflection term at the accuracy comparable with the effects of the second order is of the utmost importance for the gravitational theory and is the challenge for the 21st century fundamental physics.

The Eddington parameter $\gamma$, whose value in general relativity is unity, is perhaps the most fundamental PPN parameter, in that $(1-\gamma)$ is a measure, for example, of the fractional strength of the scalar gravity interaction in scalar-tensor theories of gravity [19]. Within perturbation theory for such theories, all other PPN parameters to all relativistic orders collapse to their general relativistic values in proportion to $(1-\gamma)$. This is why measurement of the first order light deflection effect at the level of accuracy comparable with the second-order contribution would provide the crucial information separating alternative scalar-tensor theories of gravity from GR [20] and also to probe possible ways for gravity quantization and to test modern theories of cosmological evolution [16–18].

The LATOR mission is designed to directly address the issue above with an unprecedented accuracy [21]. The test will be performed in the solar gravity field using optical interferometry between two micro-spacecraft. Precise measurements of the angular position of the spacecraft will be made using a fiber coupled multi-chanelled optical interferometer on the ISS with a 100 m baseline. The primary objective of the LATOR mission will be to measure the gravitational deflection of light by the solar gravity to accuracy of 0.1 picoradians (prad) ($\sim 0.02\ \mu$as), which corresponds to ∼10 picometers (pm) on a 100 m interferometric baseline.

A combination of laser ranging among the spacecraft and direct interferometric measurements will allow LATOR to measure deflection of light in the solar gravity by a factor of more than 3,000 better than had recently been accomplished with the Cassini spacecraft. In particular, this mission will not only measure the key PPN parameter $\gamma$ to unprecedented levels of accuracy of one part in $10^8$. As a result, this experiment will measure values of other PPN parameters such as parameter $\delta$ to 1 part in $10^3$ and discussion thereafter), the solar quadrupole moment parameter $J_2$ to 1 part in 20, and the frame dragging effects on light due to the solar angular momentum to precision of 1 parts in $10^2$.

The LATOR mission technologically is a very sound concept; all technologies that are needed for its success have been already demonstrated as a part of the JPL's Space Interferometry Mission (SIM) development. Technology that has become available in the last several years such as low cost microspacecraft, medium power highly efficient solid state and fiber lasers, and the development of long range interferometric techniques make possible an unprecedented factor of 3,000 improvement in this test of general relativity possible. This mission is unique and is the natural next step in solar system gravity experiments which fully exploits modern technologies.

This paper organized as follows: Section II provides the overview for the LATOR experiment including the preliminary mission design. In Section III we discuss the current design for the LATOR flight system. In Section IV we will discuss the expected performance for the LATOR instrument. Section V discusses the next steps that will taken in the development of the LATOR mission.

## II. OVERVIEW OF LATOR

The LATOR experiment uses laser interferometry between two micro-spacecraft whose lines of sight pass close by the Sun to accurately measure deflection of light in the solar gravity [21]. Another component of the experimental design is a long-baseline stellar optical interferometer placed on the ISS. Figure 1 shows the general concept for the LATOR missions including the mission-related geometry, experiment details and required accuracies.

We shall now discuss the LATOR mission in detail.

### A. Mission Design

As evident from Figure 1, the key element of the LATOR experiment is a redundant geometry optical truss to measure the departure from Euclidean geometry caused by gravity. Two spacecraft are injected into a heliocentric solar orbit on the opposite side of the Sun from the Earth. The triangle in figure has three independent quantities but three arms are monitored with laser metrology. In particular, each spacecraft equipped with a laser ranging system that enable a measurement of the arms of the triangle formed by the two spacecraft and the ISS. According to Euclidean rules this determines a specific angle at the interferometer; LATOR can directly measure this angle directly. In particular, the laser beams transmitted by each spacecraft are detected by a long baseline ($\sim 100$ m) optical interferometer on the ISS. The actual angle measured at interferometer is compared to angle calculated using Euclidean rules and three side measurements; the difference is the non-Euclidean deflection signal [which varies in time during spacecraft passages] which contains the scientific information. Therefore, the uniqueness of this mission comes with its built-in geometrically redundant architecture that enables LATOR to measure the departure from Euclidean geometry caused by the solar gravity field to a very high accuracy. The accurate measurement of this departure constitutes the primary mission objective.

To enable the primary objective, LATOR will place two spacecraft into a heliocentric orbit so that observa-

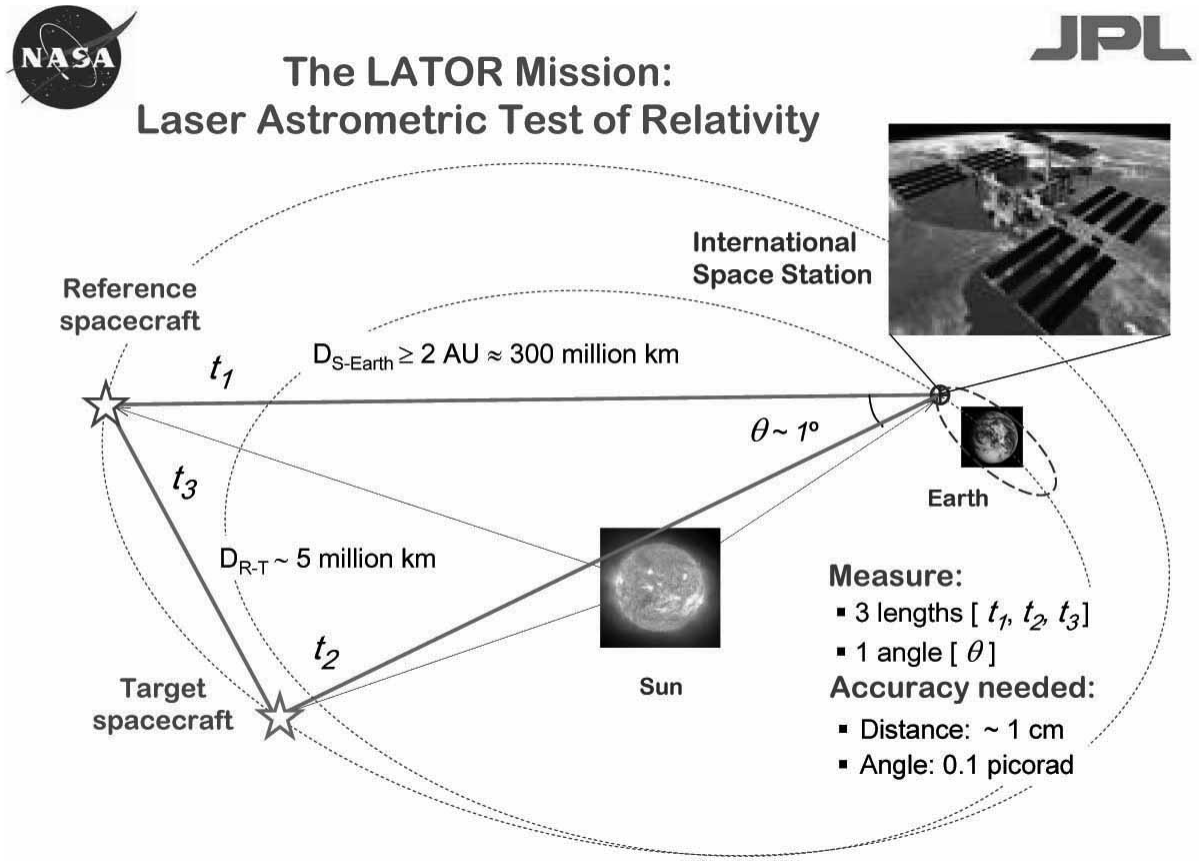


FIG. 1: The overall geometry of the LATOR experiment.

tions may be made when the spacecraft are behind the Sun as viewed from the ISS. The two spacecraft are to be separated by about 1°, as viewed from the ISS [22, 23]. With the help of the JPL Advanced Project Design Team (Team X), we recently conducted a detailed mission design studies [24]. In particular, we analyzed various trajectory options for the deep-space flight segment of LATOR, using both Orbit Determination Program (ODP) and Satellite Orbit Analysis Program (SOAP) – the two standard JPL navigation software packages.

An orbit with a 3:2 resonance with the Earth was found to uniquely satisfy the LATOR orbital requirements [24]. (The 3:2 resonance occurs when the Earth does 3 revolutions around the Sun while the spacecraft does exactly 2 revolutions of a 1.5 year orbit. The exact period of the orbit may vary slightly (<1%) from a 3:2 resonance depending on the time of launch.) For this orbit, in 13 months after the launch, the spacecraft are within $\sim 10°$ of the Sun with first occultation occuring in 15 months after launch [21]. At this point, LATOR is orbiting at a slower speed than the Earth, but as LATOR approaches its perihelion, its motion in the sky begins to reverse and the spacecraft is again occulted by the Sun 18 months after launch. As the spacecraft slows down and moves out toward aphelion, its motion in the sky reverses again and it is occulted by the Sun for the third and final time 21 months after launch.

The 3:2 Earth resonant orbit provides an almost ideal trajectory for the LATOR mission, specifically i) it imposes no restrictions on the time of launch; ii) with a small propulsion maneuver after launch, it places the two LATOR spacecraft at the distance of less then 3.5° (or $\sim 14\ R_\odot$) for the entire duration of the experiment (or ∼8 months); iii) it provides three solar conjunctions even during the nominal mission lifetime of 22 months, all within 7 month period; iv) at a cost of an extra maneuver, it offers a possibility of achieving small orbital inclinations (to enable measurements at different solar latitudes), and, finally, v) it offers a very slow change in the Sun-Earth-Probe (SEP) angle of about $\sim R_\odot$ in 4 days. As such, this orbit represents a very attractive choice for LATOR.

We intend to further study this 3:2 Earth resonant trajectory as the baseline option for the mission. In particular, there is an option to have the two spacecraft move in opposite directions during the solar conjunctions. This option will increase the amount of $\Delta v$ LATOR should carry on-board, but it significantly reduces the experiment's dependence on the accuracy of determination of the solar impact parameter. This particular option is currently being investigated and results will be reported elsewhere.

We shall now consider the basic elements of the LATOR optical design.

### B. Optical Design

A single aperture of the interferometer on the ISS consists of three 20 cm diameter telescopes (see Figure 2 for a conceptual design). One of the telescopes with a very narrow bandwidth laser line filter in front and with an InGAs camera at its focal plane, sensitive to the 1.3 $\mu$m laser light, serves as the acquisition telescope to locate the spacecraft near the Sun.

The second telescope emits the directing beacon to the spacecraft. Both spacecraft are served out of one telescope by a pair of piezo controlled mirrors placed on the focal plane. The properly collimated laser light ($\sim$10W) is injected into the telescope focal plane and deflected in the right direction by the piezo-actuated mirrors.

The third telescope is the laser light tracking interferometer input aperture which can track both spacecraft at the same time. To eliminate beam walk on the critical elements of this telescope, two piezo-electric X-Y-Z stages are used to move two single-mode fiber tips on a spherical surface while maintaining focus and beam position on the fibers and other optics. Dithering at a few Hz is used to make the alignment to the fibers and the subsequent tracking of the two spacecraft completely automatic. The interferometric tracking telescopes are coupled together by a network of single-mode fibers whose relative length changes are measured internally by a heterodyne metrology system to an accuracy of less than 10 pm.

The spacecraft are identical in construction and contain a relatively high powered (1 W), stable (2 MHz per hour $\sim$ 500 Hz per second), small cavity fiber-amplified laser at 1.3 $\mu$m. Three quarters of the power of this laser is pointed to the Earth through a 20 cm aperture telescope and its phase is tracked by the interferometer. With the available power and the beam divergence, there are enough photons to track the slowly drifting phase of the laser light. The remaining part of the laser power is diverted to another telescope, which points towards the other spacecraft. In addition to the two transmitting telescopes, each spacecraft has two receiving telescopes. The receiving telescope on the ISS, which points towards the area near the Sun, has laser line filters and a simple knife-edge coronagraph to suppress the Sun light to 1 part in $10^4$ of the light level of the light received from the space station. The receiving telescope that points to the other spacecraft is free of the Sun light filter and the coronagraph.

In addition to the four telescopes they carry, the spacecraft also carry a tiny (2.5 cm) telescope with a CCD camera. This telescope is used to initially point the spacecraft directly towards the Sun so that their signal may be seen at the space station. One more of these small telescopes may also be installed at right angles to the first one to determine the spacecraft attitude using known, bright stars. The receiving telescope looking towards the other spacecraft may be used for this purpose part of the time, reducing hardware complexity. Star trackers with this construction have been demonstrated many years ago and they are readily available. A small RF transponder with an omni-directional antenna is also included in the instrument package to track the spacecraft while they are on their way to assume the orbital position needed for the experiment.

The LATOR experiment has a number of advantages over techniques which use radio waves to measure gravitational light deflection. Advances in optical communications technology, allow low bandwidth telecommunications with the LATOR spacecraft without having to deploy high gain radio antennae needed to communicate through the solar corona. The use of the monochromatic light enables the observation of the spacecraft almost at the limb of the Sun, as seen from the ISS. The use of narrowband filters, coronagraph optics and heterodyne detection will suppress background light to a level where the solar background is no longer the dominant noise source. In addition, the short wavelength allows much more efficient links with smaller apertures, thereby eliminating the need for a deployable antenna. Finally, the use of the ISS will allow conducting the test above the Earth's atmosphere – the major source of astrometric noise for any ground based interferometer. This fact justifies LATOR as a space mission.

### C. LATOR Interferometry

In this section, we describe how angle measurements are made using the LATOR ground based interferometer. Since the spacecraft are monochromatic sources, the interferometer can efficiently use heterodyne detection to measure the phase of the incoming signal. The next section provides a simplified explanation of heterodyne interferometry for LATOR interferometer. This section also describes the use of ISS's orbit to resolve the fringe ambiguity that arises from using monochromatic signals.

#### *1. Heterodyne Interferometry*

Figures 3-5 show a simplified schematic of now angles are measured using a heterodyne interferometer. In Fig. 3, two siderostats are pointed at a target Two fiducials, shown as corner cubes, define the end points of the interferometer baseline . The light from each of the two arms is interfered with stable local oscillators (LOs) and the phase difference recorded. If the LOs in each arm were phase locked, the angles of the target with respect to the baseline normal is

$$\theta = \arcsin[\frac{(2\pi n + \phi_1 - \phi_2)\lambda}{2\pi b}] \qquad (1)$$

where $\lambda$ is the wavelength of the downlink laser, $n$ is

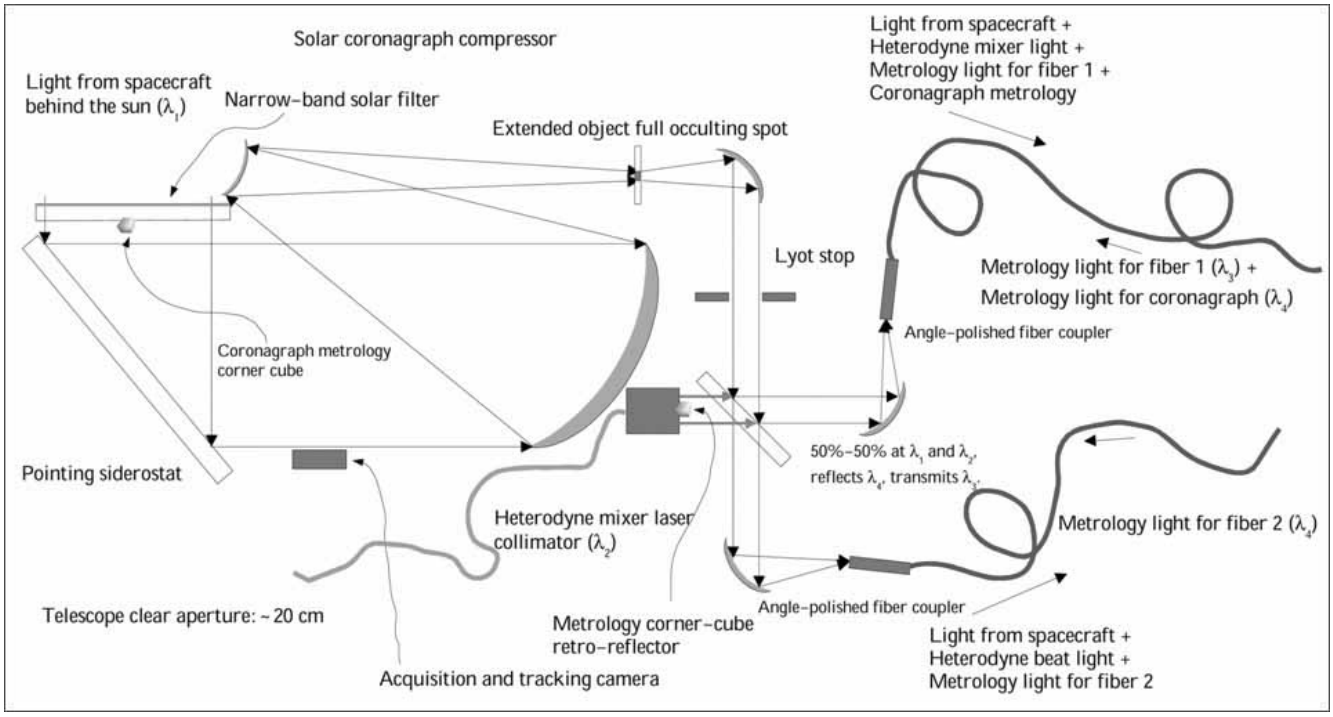


FIG. 2: Basic elements of the LATOR optical design. The laser light (together with the solar background) is going through a full aperture ($\sim$ 20cm) narrow band-pass filter with $\sim 10^{-4}$ suppression properties. The remaining light illuminates the baseline metrology corner cube and falls onto a steering flat mirror where it is reflected to an off-axis telescope with no central obscuration (needed for metrology). It is then enters the solar coronograph compressor by first going through a 1/2 plane focal plane occulter and then coming to a Lyot stop. At the Lyot stop, the background solar light is reduced by a factor of $10^6$. The combination of a narrow band-pass filter and coronograph enables the solar luminosity reduction from $V = -26$ to $V = 4$ (as measured at the ISS), thus, enabling the LATOR precision observations.

an unknown integer arising from the fringe ambiguity and $b$ is the baseline length. In order to resolve this ambiguity multiple baselines were used in the previous mission design. This is discussed in greater detail in [23]. In reality, it is difficult to phase lock the two LOs over the long baseline lengths. Figure 4 shows how a single LO can be used and transmitted to both siderostats using a single mode fiber. In this configuration, a metrology system is used to monitor changes in the path length as seen by the LO as it propagates through the fiber. The metrology system measures the distance from one beam sputter to the other. In this case, the angle is given by

$$\theta = \arcsin[\frac{(2\pi n + \phi_1 - \phi_2 + m_1)\lambda}{2\pi b}] \qquad (2)$$

where $m_l$ is the phase variations introduced by changes in the optical path of the fiber as measured by the metrology system.

Now consider the angle measurement between two spacecraft (Fig. 5). In this case the phase variations due to changes in the path through the fiber are common to both spacecraft. The differential angle is

$$\theta = \arcsin\big[\frac{(2\pi(n_1 - n_2) + (m_1 - m_2))\lambda}{2\pi b} + \\ + \frac{((\phi 1_1 - \phi 1_2) - (\phi 2_1 - \phi 2_2))\lambda}{2\pi b}\big] \qquad (3)$$

Since the spacecraft are monochromatic sources, the interferometer can efficiently use heterodyne detection to measure the phase of the incoming signal. Note that because this is a differential measurement, it is independent of the any changes in the fiber length. In reality, the interferometer will have optical paths that are different between the two spacecraft signal paths. These paths that must be monitored accurately with a metrology system to correct for phase changes in the optical system due to thermal variations. However, this metrology must only measure path lengths in each ground station and not along the entire length of the fiber. A more detailed design for the LATOR interferometer is given in Sec. III B.

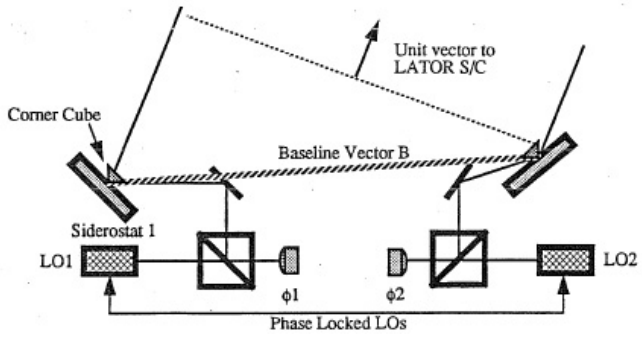


FIG. 3: Heterodyne interferometry on 1 spacecraft with phase locked local oscillator.

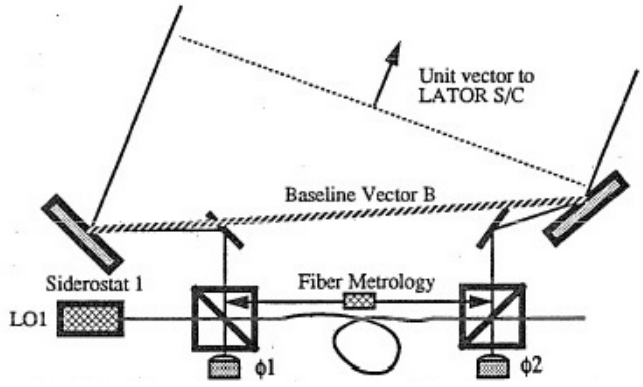


FIG. 4: Fiber-linked heterodyne interferometry and fiber metrology system.

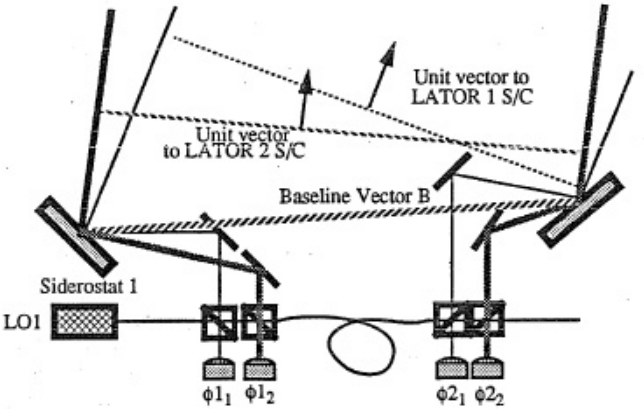


FIG. 5: Heterodyne interferometry on 2 spacecraft.

*2. Resolving the Fringe Ambiguity*

The use of multiple interferometers is a standard solution to resolve the fringe ambiguity resulting from the interferometric detection of monochromatic light [21]. The current LATOR mission proposal is immune for the fringe ambiguity problem as the orbit of the ISS provides enough variability (at least $\sim 30\%$) in the baseline projection. This variablity enables one to take multiple measurements during one orbit, in order to uniquely resolve the baseline orientation for each ISS orbit, making the fringe ambiguity not a problem for LATOR.

## III. LATOR FLIGHT SYSTEM

The LATOR flight system consists of two major components – the deep-space component that will be used to transmit and receive the laser signals needed to make the science measurements and the interferometer on the ISS that will be used to interferometrically measure the angle between the two spacecraft and to transmit and receive the laser ranging signal to each of the spacecraft.

In this Section we will discuss the design of these components in more details.

### A. LATOR Spacecraft

There are two LATOR spacecraft in the deep-space component of the mission which will be used to transmit and receive the laser signals needed to make the science measurements. Figure 6 shows a schematic of the flight system without the solar cell array. The flight system is subdivided into the instrument payload and the spacecraft bus. The instrument includes the laser ranging and communications hardware and is described in more detail in the following section. The spacecraft contains the remainder of the flight hardware which includes solar cells, attitude control, and the spacecraft structure.

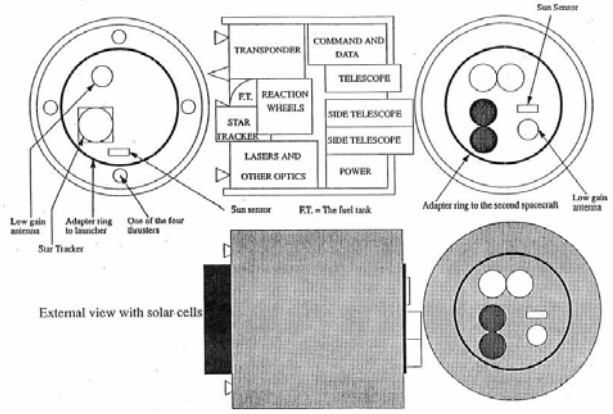


FIG. 6: LATOR spacecraft concept.

The LATOR spacecraft, like most spacecraft, will be composed of the following subsystems: thermal, structural, attitude control (ACS), power, command and data handling, telecommunications, and propulsion, in particular:

- **Thermal:** The basic thermal design will similar to that of the SA-200B, with modifications to account for the variation in range. This design uses basically passive thermal control elements with electric heaters/thermostats. The thermal control flight

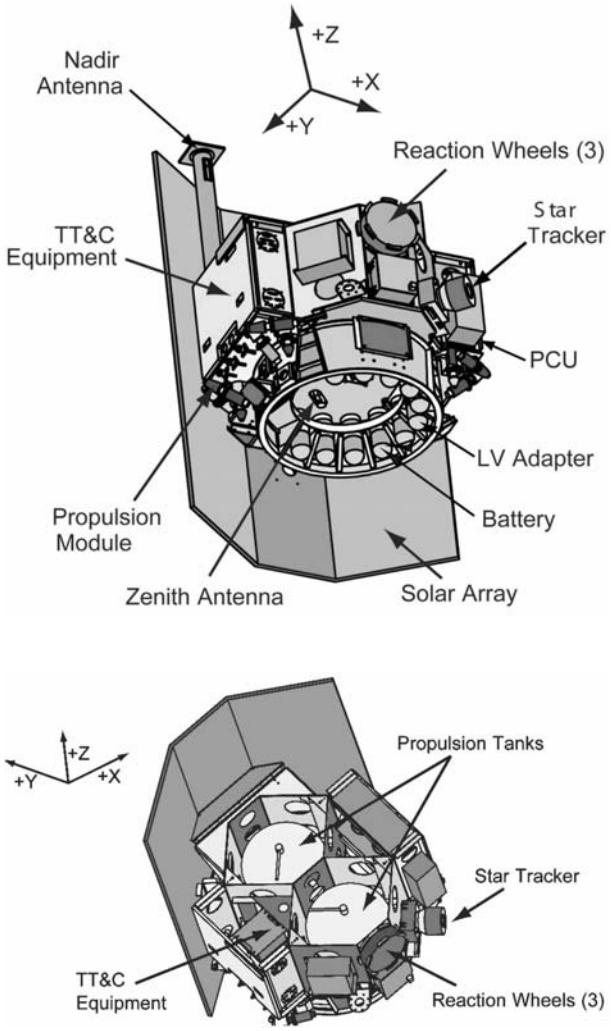


FIG. 7: A typical Spectrum Astro SA-200S/B bus. With minor modifications this configuration may be adopted for the deep-space component of the LATOR mission.

elements are multilayer insulation (MLI), thermal surfaces, thermal conduction control, and sensors. The active elements are minimized and will be only electric heaters/thermostats. To minimize heater power thermal louvers may be used. The current design assumes that spacecraft uses passive thermal control with heaters/thermostats because it is basically designed for Earth orbit.

- **Structural:** The current best estimate (CBE) for the total dry mass is 115kg including a set of required modifications to the standard SA-200B bus (i.e. a small propulsion system, a 0.5m HGA for deep-space telecom, etc.) The design calls for launching the two spacecraft side-by-side on a custom carrier structure as they should easily fit into the fairing (for instance, Delta II 2425-9.5). The total launch mass for the two spacecraft will be 552 kg. This estimate may be further reduced, given more time to develop a point design.

- **Attitude Control:** An attitude control system may be required to have pointing accuracy of 6 $\mu$rad and a pointing knowledge of 3 $\mu$rad. This may be achieved using a star tracker and sun sensor combination to determine attitude together with reaction wheels (RW) to control attitude. Cold-gas jets may be used to desaturate RWs. A Spectrum Astro SA-200B 3-axis stabilized bus with RWs for fine pointing and thrusters for RW desaturation is a good platform [24]. For the current experiment design it is sufficient to utilize a pointing architecture with the following performance (3 sigma, per axis): control 6 $\mu$rad; knowledge 3 $\mu$rad; stability 0.1 $\mu$rad/sec. The SA-200B readily accommodates these requirements.

- **Power Subsystem:** The flight system will require $\sim$50 W of power. This may be supplied by a 1 square meter GaAs solar cell array. To maintain a constant attitude with respect to the Sun, the solar cells must be deployed away from the body of the spacecraft. This will allow the cells to radiate away its heat to maintain the cells within their operating temperature range.

- **Telecommunications:** The telecommunications subsystem will be a hybrid which will utilize the optical communications capability of the instrument as the primary means of transmitting and receiving commands and data. In addition, a small low gain antenna for low data rate radio communications will be used for emergency purposes. This system will use a 15 W transmitter and 10 dB gain antenna. Using X band this system can operate with a 5 bit per second (bps) data rate. The design calls for an SDST X-Band transponder, operating at 15 W X-Band SSPA, a 0.5m HGA, two X-Band LGAs pointed opposite each other, a duplexer, two switches and coax cabling.

- **Propulsion:** The propulsion subsystem for SA-200S bus will be used as is. This will ensure a minimal amount of engineering required. System is a blowdown monopropellant system with eight 5N thrusters, two 32 cm tanks all with 22kg propellant capacity. The system exists and was tested in may applications.

### B. Interferometer on the ISS

The LATOR ground station is used to interferometrically measure the angle between the two spacecraft and to transmit and receive the laser ranging signal to each of the spacecraft. A block diagram of the laser ground station is shown in Fig. 8 and is described in more detail below. The station on the ISS is composed of a two

laser beacon stations which perform communications and laser ranging to the spacecraft and two interferometer stations which collect the downlink signal for the astrometric measurement. In addition the station uses a fiber optic link to transmit the common local oscillator to the interferometer stations.

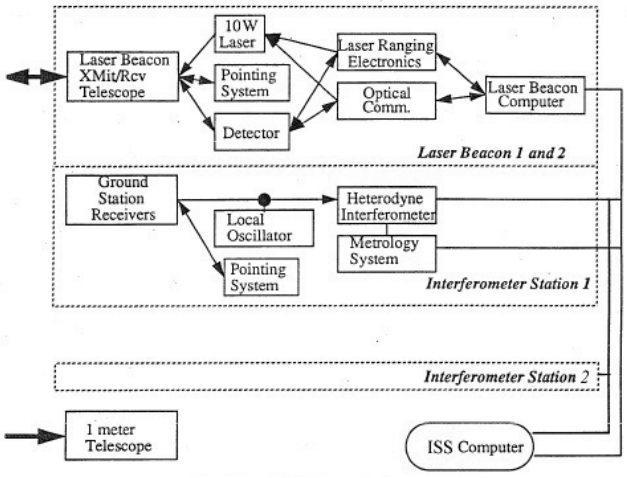


FIG. 8: LATOR station block diagram.

*Laser Beacon Station*

The laser beacon stations provide the uplink signals to the LATOR spacecraft and detect their downlink signals. The transmitter laser signal is modulated for laser ranging and to provide optical communications. Separate transmitters are used for each spacecraft each using a 1 W laser frequency doubled Nd:Yad laser at 532 nm as the source for each laser beacon. The laser beam is expanded to a diameter of 0.2 meter and is directed toward the spacecraft using a siderostat mirror. Fine pointing is accomplished with a fast steering mirror in the optical train.

During initial acquisition, the optical system of the laser beacon is modified to produce a team with a 30 arcsec divergence. This angular spread is necessary to guarantee a link with the spacecraft, albeit a weak one, in the presence of pointing uncertainties. After the acquisition sequence is complete, the beam is narrowed to a diffraction limited beam, thereby increasing the signal strength.

The downlink laser signal at 1.3 $\mu$m, is detected using a $12 \times 12$ ($10 \times 10$ arcsec) array of Germanium detectors. In order to suppress the solar background, the signal is heterodyned with a local oscillator and detected within a narrow 5 kHz bandwidth. In the initial acquisition mode, the detection system searches over a 300 MHz bandwidth and uses a spiral search over a 30 arcsec angular field to find the downlink signal. Upon acquisition, the search bandwidth is decreased to 5 kHz and a quad-cell subarray is used to point the siderostat and fast steering mirrors of the beacon.

*Interferometer Stations*

The interferometer stations collect the laser signal from both spacecraft to perform the heterodyne measurements needed for the interferometric angle measurement. There are a total of five receivers to make the four angular measurements needed to resolve fringe ambiguity.

The detection and tracking system is basically similar to the receiver arm of the laser beacon described in the previous section. Light is collected by a 0.2 meter siderostat mirror and compressed with a telescope to a manageable beam size. The light from each of the spacecraft is separated using a dual feed optical system as shown in Fig. 10. A fast steering mirror is used for high bandwidth pointing of the receiver. Each spacecraft signal is interfered with a local oscillator and the phase measurement time tagged and recorded. A $6 \times 6$ Ge array ($5 \times 5$ arcsec FOV) is used to provide heterodyne acquisition and tracking of the LATOR spacecraft.

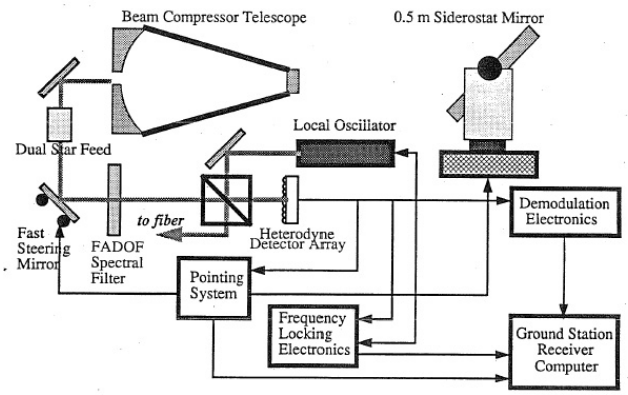


FIG. 9: Receiver on the ISS.

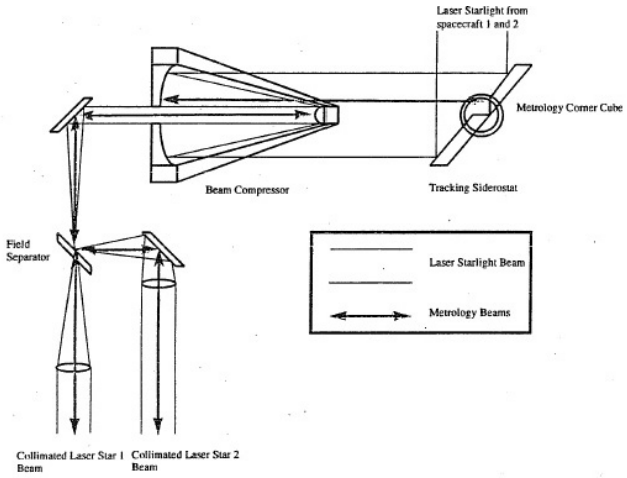


FIG. 10: Dual feed optical system.

*ISS-Based Interferometer*

Figure 11 shows a schematic of the ISS-based fiber interferometer used to perform the angular measurement between the spacecraft. A detailed description of how this interferometer makes its measurement is presented in Section II C. The interferometer includes tie heterodyne detection of the downlink signals which have been described in the previous section. The local oscillator (LO) is generated in one of the ground station receivers and is frequency locked to the laser signal from one of the spacecraft. The LO is then broadcast to the other station on the ISS through a 100 m single mode polarization preserving fiber. The heterodyne signals from all the stations (2 stations, 2 signals each) are recorded and time tagged.

Figure 11 also shows two metrology systems used in the interferometer. The first metrology system measures the difference in optical path between the two laser signal paths and is essential to proper processing of the heterodyne data. The second metrology system measures the changes in the optical path through the fiber. This measurement monitors the length of the fiber and is used in the post processing of the interferometer data. The internal path metrology system, shown in the figure, measures the paths from corner cube on the siderostat mirror (shown as two, really only one) to the metrology beam sputter. It is essential that the laser metrology system be boresighted to the laser signal path so the correct distance is measured. A Michelson interferometer with a frequency shift in one arm measure changes in the length of each signal path. Both spacecraft signal paths are measured simultaneously. This is accomplished by using an electro-optic cell and modulating each beam at a different frequency. A He-Ne laser is used as the light source for this metrology system. Filters at the output of the detector are then used to separate the signals corresponding to each metrology beam.

The fiber metrology system measures changes in the optical path through the fiber. This system uses local oscillator signal in a Michelson configuration. Figure 12 shows the correspondence between a standard Michelson interferometer and the fiber metrology system. The two X couplers serve as the beam splitters. Reflectors at the ends of the fiber couplers serve as the reference and signal mirrors. One of these reflectors is dithered to frequency shift the output signal. The phase measurement at the detector measures changes in the path length between points X1 and X2, if Ml-X1 and M2-X2 are held constant. This is accomplished by placing the X couplers and mirrors at each end of the fiber on a single thermally stable optical breadboard.

The interferometer will be formed by the two optical transponder assemblies with dimensions of approximately 0.6 m × 0.6 m × 0.6 m for each assembly (Fig. 13). The mass of each telescope assembly will be about 120 kg. The location of these packages on the ISS and their integration with the ISS's power, communication and attitude control system are given below:

- Two LATOR transponders will be physically located and integrated with the ISS infrastructure. The location will enable the straight-line separation between the two transponders of ∼100 m and will provide a clear line-of-site (LOS) path between the two transponders during the observation periods. Both transponder packages will have clear LOS to their corresponding heliocentric spacecraft during pre-defined measurement periods.

- The transponders will be physically located on the ISS structure to maximize the inherent ISS sun-tracking capability. The transponders will need to point towards the Sun during each observing period. By locating these payloads on the ISS outboard truss segments (P6 and S6 outwards), a limited degree of automatic sun-tracking capability is afforded by the alpha-gimbals on the ISS.

- The minimum unobstructed LOS time duration between each transponder on the ISS and the transponders and their respective spacecraft will be 58 minutes per the 92 min orbit of the ISS.

- The pointing error of each transponder to its corresponding spacecraft will be no greater than 1 $\mu$rad for control, 1 $\mu$rad for knowledge, with a stability of 0.1 $\mu$rad/sec, provided by combination of the standard GPS link available on the ISS and $\mu$-g accelerometers.

### C. LATOR Instrument

The LATOR instrument is used to perform laser ranging between the two spacecraft; it is also used (the second set) for laser ranging and optical communications between the spacecraft and the ISS. Figure 14 shows a block diagram of the instrument subsystems which are describe in more detail below.

- **ISS-SC Receiver/Transmitter:** The ISS/SC receiver performs the acquisition, tracking, and detection of the signals from the ISS (Figure 15). This uplinked signal will be sent at 1064 nm and will contain modulation to perform both laser ranging and to send control signals to the spacecraft. The signals from the ISS are detected by a telescope with a collecting aperture of 20 cm. A coronograph will by used to suppress stray light from the Sun. In addition a combination of a wideband interference filter and a narrow band Faraday Anomalous Dispersion Optical Filter (FADOF) will used to reject light outside a 0.005 nm band around the laser line. The incoming signal is subdivided with one portion going to a high bandwidth detector and the other to an acquisition and tracking CCD array. Using a 64 × 64 CCD array with pixels sized

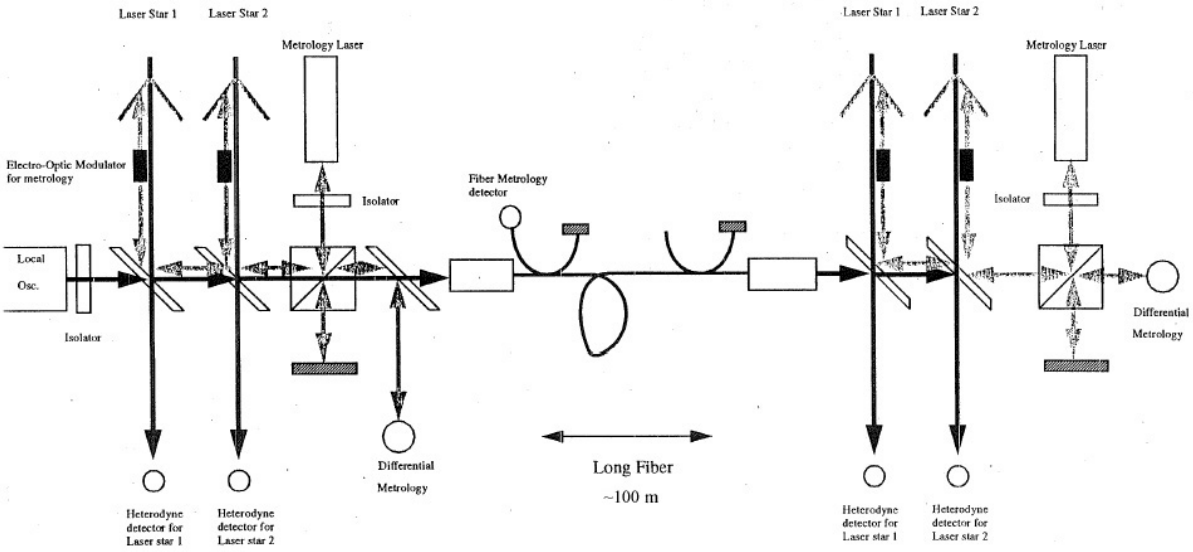


FIG. 11: ISS-based interferometer.

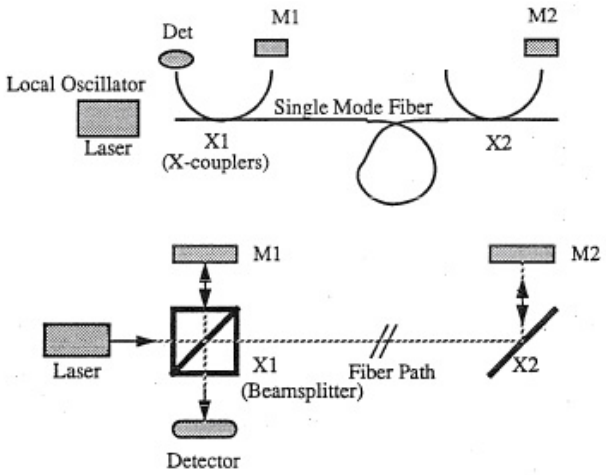


FIG. 12: Fiber metrology system.

to a diffraction limited spot, this array will have a 5 arcmin field of view which is greater than the pointing knowledge of the attitude control system and the point ahead angle (40 arcsec). After acquisition of the ISS beacon, a $2 \times 2$ element subarray of the CCD will be used as a quad cell to control the ISS-SC two axis steering mirror. This pointing mirror is common to both the receiver and transmitter channel to minimize misalignments between the two optical systems due to thermal variations. The pointing mirror will have 10 arcminute throw and a pointing accuracy of 0.5 arcsec which will enable placement of the uplink signal on the high bandwidth detector.

The ISS-SC transmitter sends a laser signal to both the interferometer collectors and the beacon receivers. The signal will be encoded for both ranging and communication information. In particular, the transmitted signal will include the inter-spacecraft ranging measurements. The transmitter uses a 2 W frequency stabilized Nd:YAG laser at 1.3 $\mu$m. A 5 kHz line width is required to simplify heterodyne detection at the ground station. A 0.15 meter telescope is used to transmit the laser beam and a steering mirror is used for pointing. The mirror uses information from the attitude control system (ACS), the quad-cell detector in the receiver, and the point ahead information from the instrument controller to determine the transmit direction. A fast steering mirror is used to maintain high bandwidth pointing control for both the transmitter and receiver.

We have also considering the possibility of using a common optical system for both the transmitter and receiver. Figure 16 shows a schematic of such a transmitter/receiver system. Because of the difference in the receive and transmit wavelengths, dichroic beam splitters and filters are used to minimize losses from the optics and leakage into the detectors. In this scheme a point ahead mirror is used maintain a constant angular offset between the received and transmitted beams. Because of the common optical elements, this system is more tolerant to misalignments than the previous configuration.

- **Inter-S/C Receiver/Transmitter:** The inter-S/C receiver/transmitter uses two separate optical systems. The receiver detects the laser ranging signal from the other spacecraft. The receiver is similar in design to the ISS-S/C receiver subsystem. Since there is no solar background contribution, the coronograph and FADOF filter have been

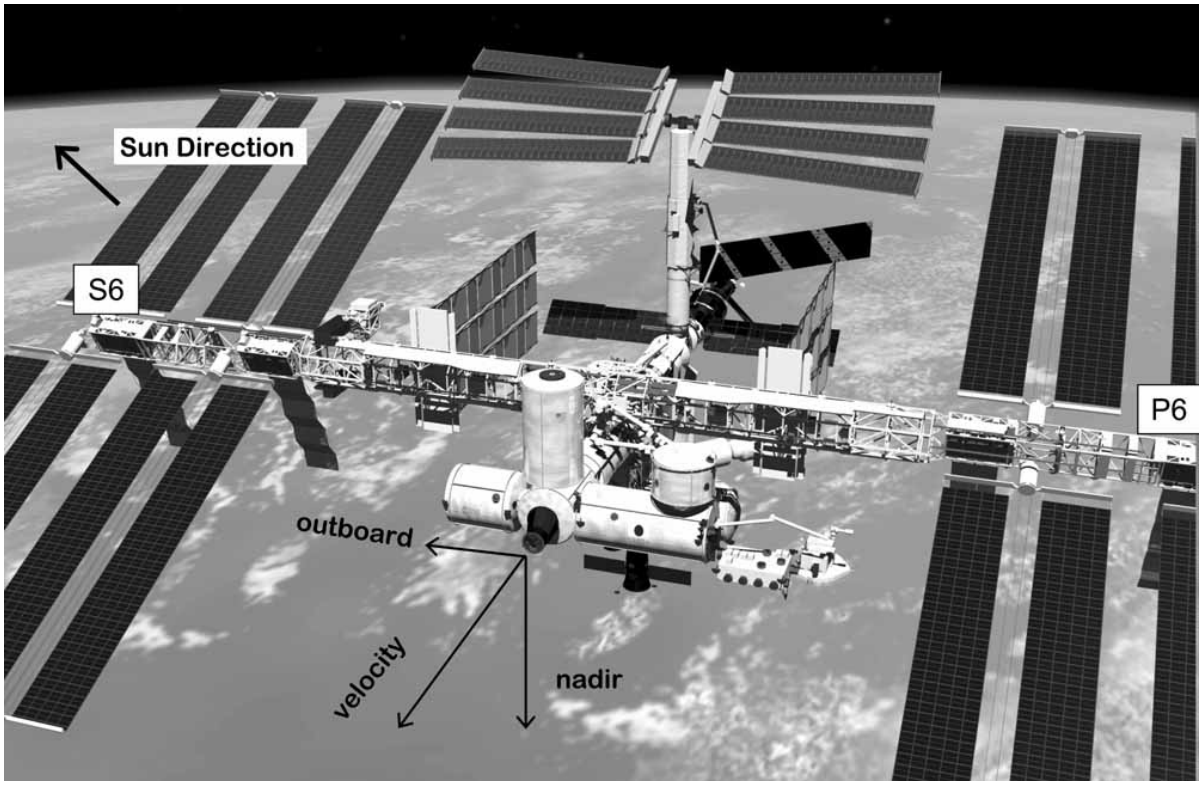


FIG. 13: Location of the LATOR interferometer on the ISS. To utilize the inherent ISS sun-tracking capability, the LATOR optical packages will be located on the outboard truss segments P6 and S6 outwards.

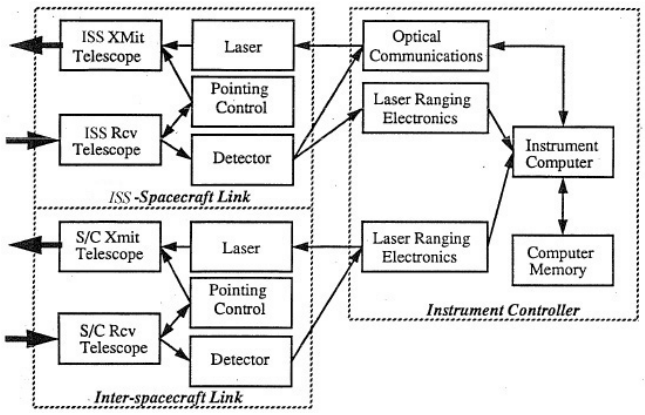


FIG. 14: LATOR instrument subsystem block diagram.

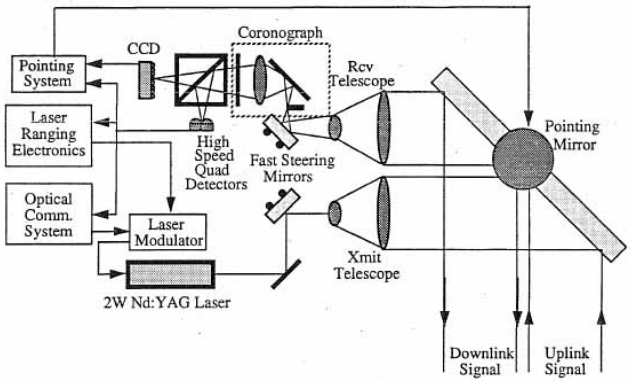


FIG. 15: S/C Transmitter & Receiver (ISS-Space Link).

removed. Detection of the signal is accomplished using a CCD for acquisition and a quad cell subarray for tracking. The tracking signal is also used to control the pointing of the transmitter minor. A separate high bandwidth detector is used for detecting the laser ranging signal.

The inter-S/C transmitter sends the laser ranging signal to the other spacecraft. The transmitter uses a 780 nm laser with an output power of 10 mW. The transmitter and receiver telescopes have an aperture of 0.1 m diameter. Because of the close proximity of the LATOR spacecraft, thermal drifts which cause misalignments between the transmitter and receiver optical systems can be sensed and corrected rapidly. In addition, the LATOR geometry requires minimal point ahead since the transverse velocity between spacecraft is nearly zero.

- **Instrument Controller:** The instrument controller subsystem contains the remainder of the instrument hardware. This includes the electronics needed for the laser ranging and optical communications as well as the computer used to control the instrument. The instrument computer will take in-

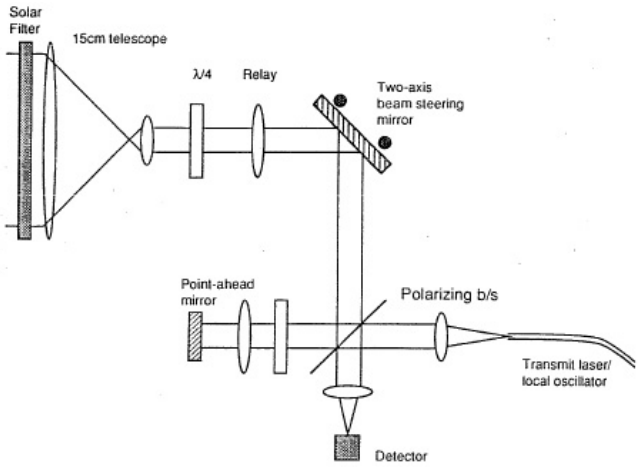


FIG. 16: ISS-S/C Link with common optics: spiral scanning spatial acquisition; open loop point ahead control with piezo actuators; fiber-coupled, frequency stabilized transmitter; pupil planes at the steering mirror and mixing apertures.

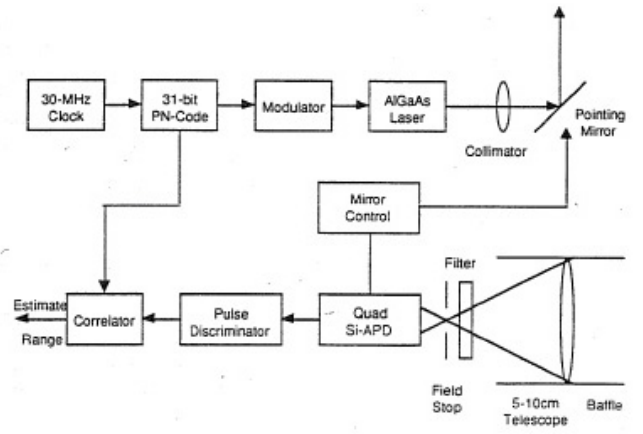


FIG. 17: ISS-S/C Link with common optics: spiral scanning spatial acquisition; open loop point ahead control with piezo actuators; fiber-coupled, frequency stabilized transmitter; pupil planes at the steering mirror and mixing apertures.

formation from the attitude control system and receiver subsystems in order to control the pointing of the transmit subsystems and the modulation of their laser signals.

The LATOR instrument in each of the two spacecraft consist of three laser metrology transmitters and receivers which can be gimbaled to point at the other spacecraft, and a camera system to acquire the incoming laser signals and to control the pointing of the outgoing beams. In addition, the instrument contains a laser ranging transponder in order to determine the spacecraft position from the ground.

- **Laser Metrology Transceiver Subsystem** The metrology transceiver consists of the laser, modulators, optics, and frequency stabilizer. The laser light is first frequency stabilized to better than 1 part in $10^{10}$, in order to make the measurements. The laser light is then frequency modulated in order to produce the heterodyne signal and distinguish between incoming and outgoing beams. Finally light is then collimated and injected into the beam launcher optics. The incoming metrology signal is received by the beam launcher optics and is interfered with the local laser. A cat's eye retroreflector serves as the spacecraft fiducial and is common to all three beam launchers.

- **Beam Launcher/Receiver Optics:** In the current instrument design, the modulated laser beam is injected using a polarization preserving single mode fiber and expanded to a 0.5 cm beam. A cat's eye retroreflector is one of several devices that can be used as the metrology fiducial and is common to the three metrology beams. The cat's eye uses two optically contacted concentric hemispheres with radius of $\sim 10$ cm and $\sim 20$ cm. The cat's eye is sized many times larger than the beam in order to minimize the effect of spherical aberration. The beam is then expanded to a 5 cm beam using a refractive telescope. A refractive design was chosen because changes in the optical path are relatively insensitive to changes in the position and orientation of the optical elements.

- **Acquisition Camera (AC) Subsystem:** AC that will be used as the sensor for pointing the metrology beam. In the previous study the $512 \times 512$ camera was used to detect the position of the incoming laser beam to 0.5 arcsec over a 1 degree field by interpolating the centroid of the spot to 0.1 pixel. Three cameras were used to track each of the incoming metrology beams. The outgoing laser beam was retroreflected from the alignment corner cube to produce a spot on the acquisition camera on which to servo the pointing gimbal.

- **Pointing Subsystem:** In the current instrument design the entire beam launcher optical assembly is gimbaled to point the metrology beam to the target spacecraft. The 2-axis gimbal has a center of rotation at the center of the cat's eye retro reflector. This optical arrangement measures the distance between the optical fiducials and is not sensitive to slight misalignments to first order. The gimbal will have a range of 1 degree and a pointing resolution of 0.5 arcsec.

### D. LATOR Operations

This section describes the sequence of events that lead to the signal acquisition and that occurs during each observation period. This sequence will be initiated at the beginning of the experiment period, after ISS emergence

from the Earth's shadow. It assumed that boresighting of the spacecraft attitude with the spacecraft transmitters and receivers have already been accomplished. This sequence of operations is focused on establishing the ISS to spacecraft link. The interspacecraft link is assumed to be continuously established after final-deployment (at $\sim 15^\circ$ off the Sun), since the spacecraft never lose line of sight with one another.

The laser beacon transmitter at the ISS is expanded to have a beam divergence of 30 arcsec in order to guarantee illumination of the LATOR spacecraft. After reemerging from the Earth's shadow this beam is transmitted to the craft and reaches them in about 18 minutes. At this point, the LATOR spacecraft acquire the expanded laser beacon signal. In this mode, a signal-to-noise ratio (SNR) of 4 can be achieved with 30 seconds of integration. With an attitude knowledge of 10 arcsec and an array field of view of 30 arcsec no spiral search is necessary. Upon acquisition, the receiver mirror on the spacecraft will center the signal and use only the center quad array for pointing control. Transition from acquisition to tracking should take about 1 minute. Due to the weak uplink intensity, at this point, tracking of the ISS station is done at a very low bandwidth. The pointing information is fed-forward to the spacecraft transmitter pointing system and the transmitter is turned on. The signal is then re-transmitted down to the ISS with a light-travel time of 18 minutes.

Each interferometer station and laser beacon station searches for the spacecraft laser signal. The return is heterodyned with using an expanded bandwidth of 300 MHz. In this case, the solar background is the dominant source of noise, and an SNR ratio of 5 is achieved with 1 second integration. Because of the small field of view of the array, a spiral search will take 30 seconds to cover a 30 arcsec field. Upon acquisition, the signal will be centered on the quad cell portion of the array and the local oscillator frequency locked to the spacecraft signal. The frequency band will then be narrowed to 5 kHz. In this regime, the solar background is no longer the dominant noise source and an SNR of 17.6 can be achieved in only 10 msec of integration. This will allow one to have a closed loop pointing bandwidth of greater than 100 Hz and be able to compensate for the tilt errors introduced by the atmosphere. The laser beacon transmitter will then narrow its beam to be diffraction limited ($\sim$1 arcsec) aid point toward the LATOR spacecraft. This completes the signal acquisition phase, the entire architecture is in-lock and transmits scientific signal. This procedure is re-established during each 92-minute orbit of the ISS.

In the next section we will consider the LATOR preliminary astrometric error budget.

## IV. ASTROMETRIC PERFORMANCE

In our design considerations we address two types of instrumental errors, namely the offset and scale errors. Thus, in some cases, when a measured value has a systematic offset of a few pm, there are may be instrumental errors that lead to further offset errors. There are many sources of offset (additive) errors caused by imperfect optics or imperfectly aligned optics at the pm level; there also many sources for scale errors. We take a comfort in the fact that, for the space-based stellar interferometry, we have an ongoing technology program at JPL; not only this program has already demonstrated metrology accurate to a sub-pm level, but has also identified a number of the error sources and developed methods to either eliminate them or to minimize their effect at the required level.

The second type of error is a scale error. For instance, in order to measure $\gamma$ to one part in $10^8$ the laser frequency also must be stable to at least to $10^{-8}$ long term; the lower accuracy would result in a scale error. The measurement strategy adopted for LATOR would require the laser stability to only $\sim$1% to achieve accuracy needed to measure the second order gravity effect. Absolute laser frequency must be known to $10^{-9}$ in order for the scaling error to be negligible. Similarly robust solutions were developed to address the effects of other known sources of scale errors.

There is a considerable effort currently underway at JPL to evaluate a number of potential errors sources for the LATOR mission, to understand their properties and establish methods to mitigate their contributions. (A careful strategy is needed to isolate the instrumental effects of the second order of smallness; however, our experience with SIM [25–27] is critical in helping us to properly capture their contribution in the instrument models.) The work is ongoing, this is why the discussion below serves for illustration purposes only. We intend to publish the corresponding analysis and simulations in the subsequent publications.

### A. Optical Performance

The laser interferometers use $\sim$2W lasers and $\sim$20 cm optics for transmitting the light between spacecraft. Solid state lasers with single frequency operation are readily available and are relatively inexpensive. For SNR purposes we assume the lasers are ideal monochromatic sources (with $\lambda = 1.3$ $\mu$m). For simplicity we assume the lengths being measured are $2\mathrm{AU} = 3 \times 10^8$ km. The beam spread is estimated as $\sim 1$ $\mu$m/20 cm $= 5$ $\mu$rad (1 arcsec). The beam at the receiver is $\sim$1,500 km in diameter, a 20 cm receiver will detect $1.71 \times 10^2$ photons/s assuming 50% q.e. detectors. Given the properties of the CCD array it takes about 10 s to reach the desirable SNR of $\sim 2000$ targeted for the detection of the second order effects. In other words, a 5 pm resolution needed for a measurement of the PPN parameter $\gamma$ to the accuracy of one part in $\sim 10^8$ is possible with $\approx 10$ s of integration.

As a result, the LATOR experiment will be capable of measuring the angle between the two spacecraft to

TABLE I: LATOR Mission Summary: Science Objectives

| |
|---|
| • To search for cosmological remnants of scalar field in the solar system. |
| • To access the most intense gravitational environment in the solar system and test a number of dynamical scenarios in this new field-strength regime. |
| • To measure the key Eddington parameter $\gamma$ with accuracy of 1 part in $10^8$, a factor of 3,000 improvement in the tests of gravitational light deflection. |
| • To directly measure the PPN parameter $\beta$ to $\sim 1\%$ accuracy |
| • To measure effect of the second order light deflection with accuracy of $\sim 1 \times 10^{-3}$, including first ever measurement of the PPN parameter $\delta$. |
| • To measure the solar quadrupole moment (using the theoretical value of the solar quadrupole moment $J_2 \simeq 10^{-7}$) to 1 part in 20. |
| • To directly measure the frame dragging effect on the light with $\sim 1 \times 10^{-2}$ accuracy. |

$\sim 0.05$ prad, which allows light deflection due to gravitational effects to be measured to one part in $10^8$. Measurements with this accuracy will lead to a better understanding of gravitational and relativistic physics.

In our analysis we have considered various potential sources of systematic error. This information translates to the expected accuracy of determination of the differential interferometric delay of $\sim \pm 5.4$ pm, which translates in the measurement of the PPN parameter $\gamma$ with accuracy of $\sigma_\gamma \sim 0.9 \times 10^{-8}$. This expected instrumental accuracy is clearly a very significant improvement compared to other currently available techniques. This analysis serves as the strongest experimental motivation to conduct the LATOR experiment.

### B. Expected Measurement Accuracy

Here we summarize our estimates of the expected accuracy in measurement of the relativistic parameters of interest. The first order effect of light deflection in the solar gravity caused by the solar mass monopole is $\alpha_1 = 1.75$ arcsec; this value corresponds to an interferometric delay of $d \simeq b\alpha_1 \approx 0.85$ mm on a $b = 100$ m baseline. Using laser interferometry, we currently able to measure distances with an accuracy (not just precision but accuracy) of $\leq 1$ pm. In principle, the 0.85 mm gravitational delay can be measured with $10^{-9}$ accuracy versus $10^{-5}$ available with current techniques. However, we use a conservative estimate of 10 pm for the accuracy of the delay which would lead to a single measurement of $\gamma$ accurate to 1 part in $10^8$ (rather than 1 part in $10^9$), which would be already a factor of 3,000 accuracy improvement when compared to the recent Cassini result [15].

Furthermore, we have targeted an overall measurement accuracy of 10 pm per measurement, which for $b = 100$ m this translates to the accuracy of 0.1 prad $\simeq 0.02$ $\mu$as. With 4 measurements per observation, this yields an accuracy of $\sim 5.8 \times 10^{-9}$ for the first order term. The second order light deflection is approximately 1700 pm and with 10 pm accuracy and the adopted measurement strategy it could be measured with accuracy of $\sim 2 \times 10^{-3}$, including first ever measurement of the PPN parameter $\delta$. The frame dragging effect would be measured with $\sim 1 \times 10^{-2}$ accuracy and the solar quadrupole moment (using the theoretical value of the solar quadrupole moment $J_2 \simeq 10^{-7}$) can be modestly measured to 1 part in 20, all with respectable SNRs (see Table I).

The final error would have contributions from multiple measurements of the light triangle's four attributes (to enable the redundancy) taken by range and interferometer observations at a series of times. The corresponding errors will be combined with those from orbital position and velocity coordinate uncertainty. These issues are currently being investigated in the mission covariance analysis; the detailed results of this analysis will be reported elsewhere. However, our current understanding of the expected mission and instrumental accuracies suggests that LATOR will offer a very significant improvement compare to any other available techniques. This conclusion serves as the strongest experimental motivation to conduct the LATOR experiment.

## V. CONCLUSIONS

Concluding, we would like to summarize the most significant results of our LATOR mission study. The most natural question is "Why is LATOR potentially orders of magnitude more sensitive and less expensive?"

First of all, there is a significant advantage in using optical wavelengths as opposed to the microwaves – the present navigational standard. This is based on the fact that solar plasma effects decrease as $\lambda^2$ and, in the case of LATOR, we gain a factor of $10^{10}$ reduction in the solar plasma optical path fluctuations by simply moving from $\lambda = 10$ cm to $\lambda = 1$ $\mu$m. Another LATOR's advantage is its independence of a drag-free technology. In addition, the use of a redundant optical truss offers an excellent alternative to an ultra-precise orbit determination. This feature also makes LATOR insensitive to spacecraft buffeting from solar wind and solar radiation pressure.

Furthermore, the use of existing technologies, laser components and spacecraft make this mission a low cost experiment. Thus, 1 W lasers with sufficient frequency stability and $> 10$ years lifetime already developed for optical telecom and also are flight qualified for SIM. Additionally, small optical apertures $\sim$10-20cm are sufficient and provide this experiment with a high signal-to-noise ratio. There also a significant advantage in using components with no motorized moving parts. This all makes LATOR an excellent candidate for the next flight experiment in fundamental physics. Table I summarizes the science objectives for this mission.

The LATOR mission aims to carry out a test of the curvature of the solar system's gravity field with an accuracy better than 1 part in $10^8$. In spite of the previous space missions exploiting radio waves for tracking the spacecraft, this mission manifests an actual breakthrough in the relativistic gravity experiments as it allows to take full advantage of the optical techniques that recently became available. The LATOR experiment has a number of advantages over techniques that use radio waves to measure gravitational light deflection. The optical technologies allows low bandwidth telecommunications with the LATOR spacecraft. The use of the monochromatic light enables the observation of the spacecraft almost at the limb of the Sun. The use of narrowband filters, coronagraph optics and heterodyne detection will suppress background light to a level where the solar background is no longer the dominant noise source. The short wavelength allows much more efficient links with smaller apertures, thereby eliminating the need for a deployable antenna. Finally, the use of the ISS enables the test above the Earth's atmosphere – the major source of astrometric noise for any ground based interferometer. This fact justifies LATOR as a space mission.

The LATOR mission will utilize several technology solutions that recently became available. In particular, signal acquisition on the solar background will be done with a full-aperture narrow band-pass filer and coronagraph. The issue of the extended structure vibrations of the will be addressed by using $\mu$-g accelerometers. (The use of the accelerometers was first devised for SIM, but at the end their utilization is not needed. The Keck Interferometer uses accelerometers extensively.) Finally, the problem of monochromatic fringe ambiguity that complicated the design of the previous version of the experiment [23] and led to the use of variable baselines lengths – is not an issue for LATOR. This is because the orbital motion of the ISS provides variable baseline projection that eliminates this problem for LATOR.

The LATOR experiment technologically is a very sound concept; all technologies that are needed for its success have been already demonstrated as a part of the JPL's interferometry program. The LATOR experiment does not need a drag-free system, but uses a geometric redundant optical truss to achieve a very precise determination of the interplanetary distances between the two micro-spacecraft and a beacon station on the ISS. The interest of the approach is to take advantage of the existing space-qualified optical technologies leading to an outstanding performance in a reasonable mission development time. The availability of the ISS makes this mission concept realizable in the very near future; the current mission concept calls for a launch as early as in 2011 at a cost of a NASA MIDEX mission.

This mission may become a 21st century version of Michelson-Morley experiment in the search for a cosmologically evolved scalar field in the solar system. As such, LATOR will lead to very robust advances in the tests of fundamental physics: it could discover a violation or extension of GR, or reveal the presence of an additional long range interaction in the physical law. There are no analogs to the LATOR experiment; it is unique and is a natural culmination of solar system gravity experiments.

### Acknowledgments

The work described here was carried out at the Jet Propulsion Laboratory, California Institute of Technology, under a contract with the National Aeronautics and Space Administration.

[1] I.I. Shapiro, C.C.Counselman, III, and R.W. King, Phys. Rev. Lett. **36**, 555 (1976).
[2] R.D. Reasenberg et al., ApJ Lett. **234**, L219 (1979).
[3] I.I. Shapiro, et al., JGR **82**, 4329 (1977).
[4] J. D. Anderson et al., BAAS **34**, 833 (2002).
[5] D.S. Robertson, W.E. Carter and W.H. Dillinger, Nature **349** 768 (1991).
[6] D.E. Lebach et al., Phys. Rev. Lett. **75**, 1439 (1995).
[7] S. S. Shapiro, et al., Phys. Rev. Lett. **92**, 121101 (2004).
[8] K. Nordtvedt, Jr., Phys. Rev. **170**, 1186 (1968).
[9] K. Nordtvedt, Jr., Phys. Rev. D **43**, 10 (1991).
[10] K. Nordtvedt, Jr., CQG **16**, A101 (1999).
[11] K. Nordtvedt, Jr., [gr-qc/0301024].
[12] J. G. Williams, X. X. Newhall, and J. O. Dickey, Phys. Rev. D **53**, 6730 (1996).
[13] J. G. Williams et al., BAAS **33**, 836 (2001).
[14] J. G. Williams, S. G. Turyshev, D. H. Boggs, To be published Phys. Rev. Lett., 2004.
[15] B. Bertotti, L. Iess, and P. Tortora, Nature **425**, 374 (2003).
[16] T. Damour, K. Nordtvedt, Jr., Phys. Rev. Lett. **70**, 2217 (1993); Phys. Rev. D **48**, 3436 (1993).
[17] T. Damour, A. M. Polyakov, GRG **26**, 1171 (1994); Nucl. Phys. B **423**, 532 (1994).
[18] T. Damour, F. Piazza, and G. Veneziano, Phys. Rev. Lett. **89**, 081601, (2002) [gr-qc/0204094]; Phys. Rev. D **66**, 046007, (2002) [hep-th/0205111].
[19] T. Damour, G. Esposito-Farese, Phys. Rev. D **53** 5541

(1996); Phys. Rev. D **54**, 1474 (1996);
[20] K. Nordtvedt, Jr., ApJ **320**, 871 (1987).
[21] S. G. Turyshev, M. Shao, and K.L. Nordtvedt, Jr., CQG **21**, 2773 (2004), gr-qc/0311020
[22] A version of LATOR with a ground-based receiver was proposed in 1994 and performed under NRA 94-OSS-15 [23]. Due to atmospheric turbulence and seismic vibrations that are not common mode to the receiver optics, a very long baseline interferometer (30 km) was proposed. This interferometer could only measure the differential light deflection to an accuracy of 0.1 $\mu$as, with a spacecraft separation of less than 1 arc minutes.
[23] J. Yu, et al., SPIE 2200, 325 (1994); M. Shao et al., *Laser Astrometric Test of Relativity (LATOR) Mission*. JPL Technical Memorandum (1996).
[24] A. Gerber et al., *LATOR 2003 Mission Analysis*, JPL Advanced Project Design Team (Team X) Report #X-618 (2003).
[25] M. Milman, J. Catanzarite, and S. G. Turyshev, Applied Optics **41** 4884 (2002)
[26] S. G. Turyshev, Applied Optics **42**, 71 (2003) [physics/0301026]
[27] M. Milman, S. G. Turyshev, Optical Engeneering **42**, 1873 (2003) [physics/0301047]

# LATOR Spacecraft Orbits

**Kenneth Nordtvedt**
**Northwest Analysis ---- Bozeman, Montana**
**kennordtvedt@imt.net**

**In order to reach $10^{-8}$ or $10^{-9}$ precision in measurement of PPN $\gamma$,**
**LATOR's light triangle must be transversely located**
**relative to the Sun with a precision of 1 to 10 meters,**
**or scientific data must be desensitized to a greater uncertainty.**
**Spacecraft orbits can be designed to achieve this error reduction.**

The LATOR mission aims to make a major advance in the precision of testing for scalar field modifications of general relativity's pure tensor gravity. By using a laser interferometer to measure one angle of a light triangle, and laser ranging to measure the three sides of the triangle, and shaping the triangle so that two of its sides have the laser light pass close by the Sun, first-order gravitational deflection of light will be measured to part-in-a-hundred million precision. But such an accurate measurement of the theory's predictions would seem to require a correspondingly accurate knowledge of the light trajectories' impact parameters passing the Sun. This amounts to 10 meter or better knowledge of the light triangle's key transverse location coordinate.

My study deals with this issue: How can the LATOR mission succeed in meeting its goals if traditional tracking and drag-free system methods cannot supply the better than 10 meter knowledge of spacecraft location in this key long-track direction and over the several-day time interval during which the mission's key data will be taken?

**Figure 1.**

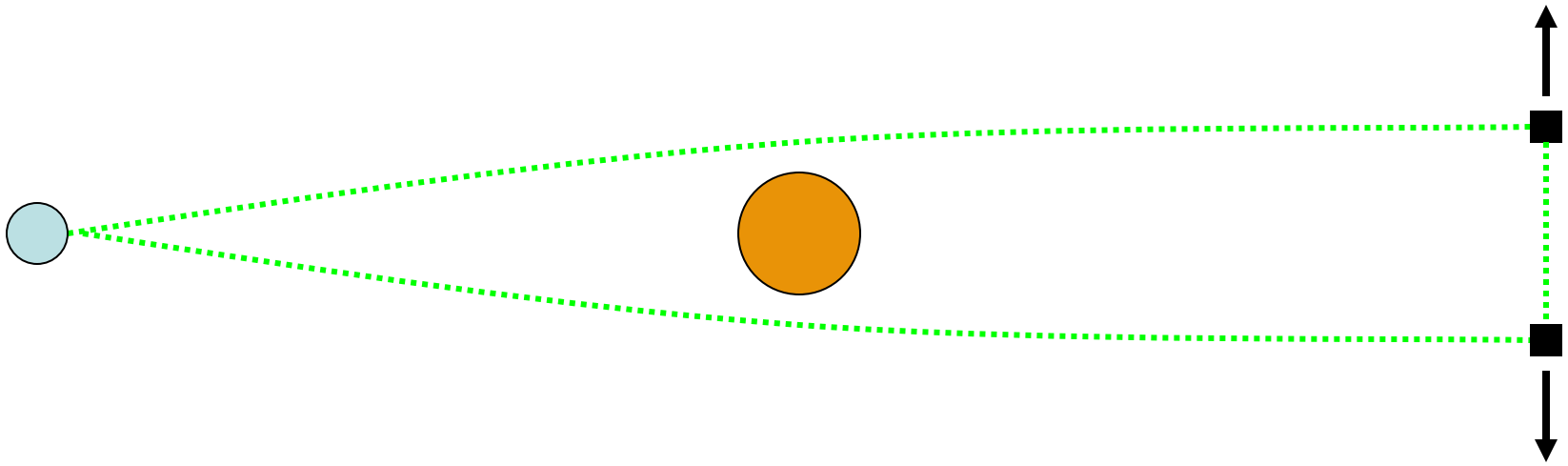

$$\theta \simeq 2\left(1+\gamma\right)\frac{GM}{c^2}\left(\frac{1}{D_A(t)}+\frac{1}{D_B(t)}\right)$$ **Doubles Experimental Sensitivity**

**Spacecraft along-track "common mode" uncertainty** $\delta Y_C = \delta\left(y_A(t)+y_B(t)\right)/2$

$$\delta\theta \simeq 2\left(1+\gamma\right)\frac{GM}{c^2}\left(\frac{1}{D_A^2}-\frac{1}{D_B^2}\right) \quad \int_0^t dt' \int_0^{t'} \ddot{Y}_C dt''$$ **Nullified for** $D_A \simeq D_B$

Figure 1. (above) shows the mission's orbital configuration that was found to solve this challenge. When the two spacecraft making up two corners of the light triangle pass by the Sun as viewed from the third corner of the light triangle near Earth, the spacecraft's angular positions from the Sun should be about equal and opposite.

Figure 2. (below) shows the view from Earth during the key period of days during which the important light deflection data is taken. One benefit of this orbital configuration is that the deflection angles of the light from the two spacecraft add together to double the scientific signal and thereby the experiment's sensitivity.

**Figure 2.**

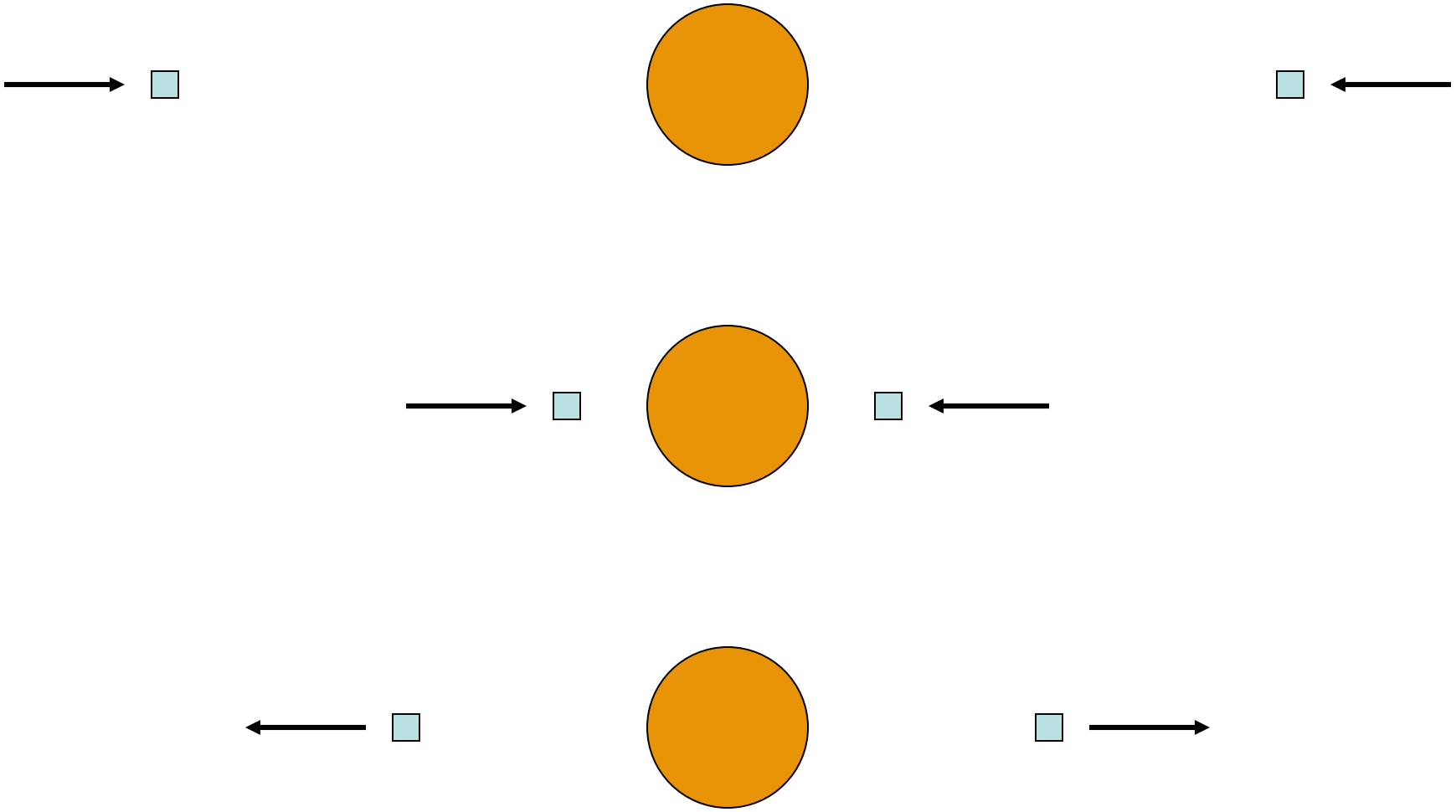

But more importantly, this configuration leads to the scientifically interesting deflection angle being insensitive in linear order to the uncertainties in the transverse location of the light triangle.  This results because one deflection angle increases while the other deflection angle decreases by equal amount in proportion to this key uncertainty.  The 10-meter knowledge requirement can be substantially relaxed!

In Figure 3. below the three main deflection signals of interest are shown in their analytic form as function of light impact parameter distances - first-order monopolar light deflection, gravity's non-linear second-order monopolar light deflection, and the light deflection proportional to the Sun's Newtonian quadrupole moment.

**Figure 3.**

## Scientific Signals in Angle Deflection

$$\Theta \simeq 2\left(1+\gamma\right)\frac{GM_S}{c^2}\left(\frac{1}{D_A}+\frac{1}{D_B}\right) \quad + \quad \chi\left(\frac{GM_S}{c^2}\right)^2\left(\frac{1}{D_A^2}+\frac{1}{D_B^2}\right)$$

$$+ \quad \left(1+\gamma\right)J_2\frac{GM_S a_S^2}{c^2}\left(\frac{1}{D_A^3}+\frac{1}{D_B^3}\right) \quad + \quad ....$$

**with modifications $F_n\left(L\right)$ for spacecraft at solar latitude $L$**

In Figure 4. the general features are shown of the spacecraft orbits from the time they leave Earth up to the times when their positions as seen from Earth pass behind or close by the Sun.  The first major maneuver puts the spacecraft on a 1.5-year period orbit; then later, an additional impulse is given to just one of the spacecraft that results in the later occurrence of the desired orbital configuration - equal but opposite relative motion of the spacecraft lines of sight relative to the Sun.

**Figure 4.**

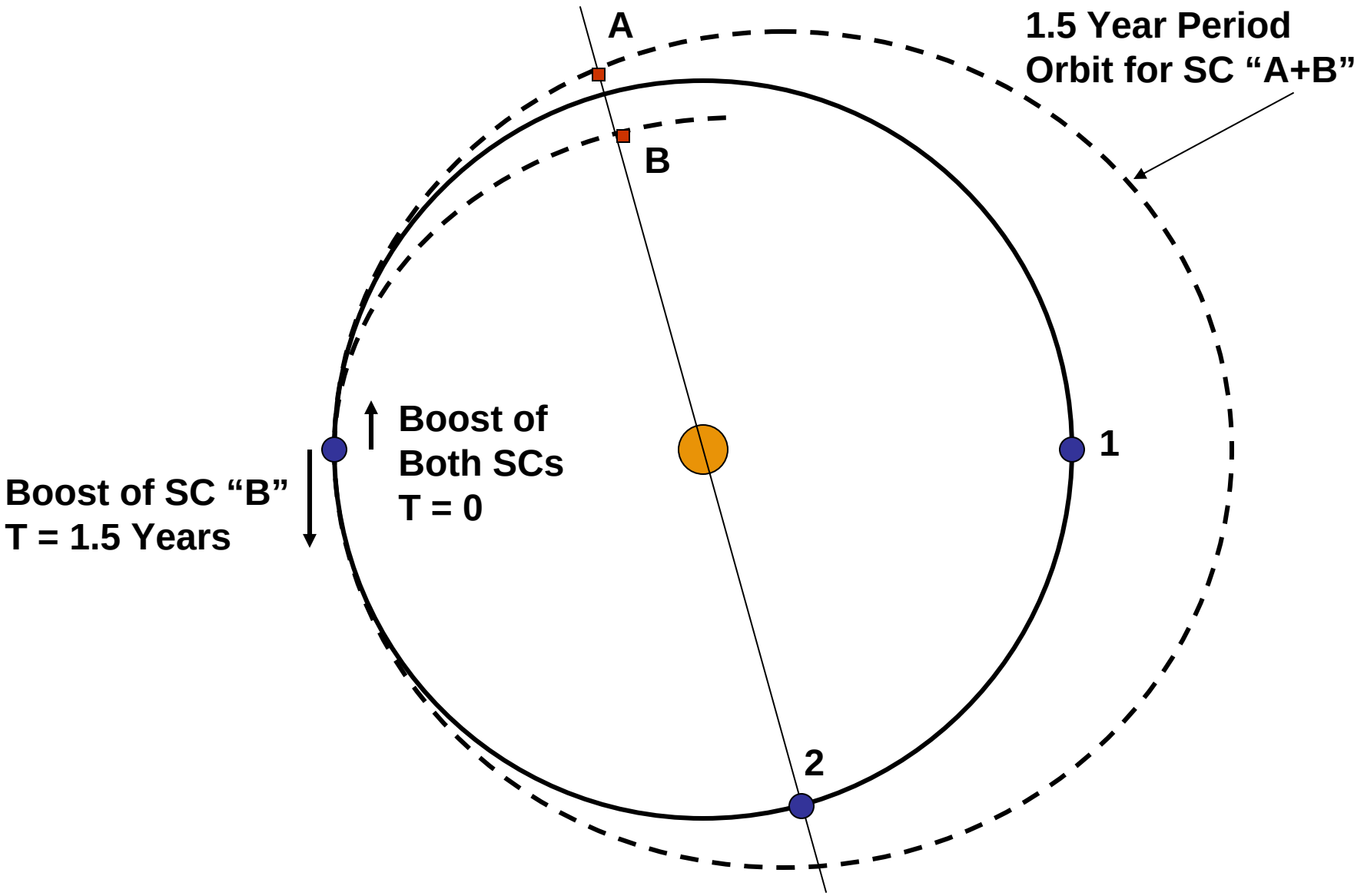
A
B
1.5 Year Period
Orbit for SC “A+B”
Boost of
Both SCs
T = 0
Boost of SC “B”
T = 1.5 Years
1
2

**Figure 5.**

# Model Fitting Issues

$$\Theta = 2\left(1+\gamma\right)\frac{GM_S}{c^2}\left(\frac{1}{d/2+D^{(CM)}}+\frac{1}{d/2-D^{(CM)}}\right) \quad + \quad \chi \text{ and } J_2 \text{ signals}$$

$$d = D_A + D_B \quad \text{is well-measured by light triangle}$$

$$D^{(CM)} = \left(D_A - D_B\right)/2 = D(t_0)^{(CM)} + \dot{D}(t_0)^{(CM)}\left(t-t_0\right) + \int_{t_0}^{t} dt' \int_{t_0}^{t'} \delta a^{(CM)} dt''$$

$$\frac{\partial\Theta}{\partial\gamma} = 2\frac{GM_S}{c^2}\left(\frac{1}{D_A(t)}+\frac{1}{D_B(t)}\right) \qquad \frac{\partial\Theta}{\partial\chi} = \left(\frac{GM_S}{c}\right)^2\left(\frac{1}{D_A^2}+\frac{1}{D_B^2}\right) \quad ....$$

$$\frac{\partial\Theta}{\partial D^{(CM)}} = 2\left(1+\gamma\right)\frac{GM_S}{c^2}\left(\frac{1}{D_A^2}-\frac{1}{D_B^2}\right) \qquad \frac{\partial\Theta}{\partial\dot{D}^{(CM)}} = \frac{\partial\Theta}{\partial D^{(CM)}}\left(t-t_0\right)$$

$$\delta\Theta = \frac{\partial\Theta}{\partial D^{(CM)}} \int_{t_0}^{t} dt' \int_{t_0}^{t'} \delta a^{(CM)} dt''$$

In Figure 5. the several signal "partials" are derived to show that they have dependence on the time of observation. This dependence permits the different key parameters of the experiment to be simultaneously and independently measured by a least-squares-type fit of the mission's data. These key fit-for parameters will include the initial impact parameter and its initial time derivative at one fiducial time point in the experiment. The accelerative evolution of this impact parameter due to gravity will be well determined from our knowledge of gravity, and the accelerative evolution of this impact parameter due to drag forces on the spacecraft will have been eliminated as crucial error sources because of the special orbital configuration previously discussed.

# Controlled Antihydrogen Propulsion for NASA's Future in Very Deep Space[1]

**Michael Martin Nieto[a], Michael H. Holzscheiter[b], and Slava G. Turyshev[c]**

[a] *Theoretical Division (MS-B285), Los Alamos National Laboratory, University of California, Los Alamos, NM 87545*

[b] *Pbar Labs, LLC, 1601 Dove Street, Suite 170, Newport Beach, CA 92660*

[c] *Jet Propulsion Laboratory, California Institute of Technology, 4800 Oak Grove Drive, Pasadena, CA 91109*

**Abstract**

To world-wide notice, in 2002 the ATHENA collaboration at CERN (in Geneva, Switzerland) announced the creation of on the order of 100,000 low energy antihydrogen atoms. Thus, the idea of using condensed antihydrogen as a low-weight, powerful fuel (i.e., it produces a thousand times more energy per unit weight of fuel than fission/fusion) for very deep space missions (the Oort cloud and beyond) had reached the realm of conceivability. We briefly discuss the history of antimatter research and focus on the technologies that must be developed to allow a future use of controlled, condensed antihydrogen for propulsion purposes. We emphasize that a dedicated antiproton source (the main barrier to copious antihydrogen production) must be built in the US, perhaps as a joint NASA/DOE/NIH project. This need arises because the only practical sources in the world are at CERN and at the proposed facility at GSI in Germany. We outline the scope and magnitude of such a dedicated national facility and identify critical project milestones. We estimate that, starting with the present level of knowledge and assuming multi-agency support, the goal of using antihydrogen for propulsion purposes may be accomplished in $\sim 50$ years.

# 1 Introduction

In this century, the development of missions to deeper and deeper space will become an ever-increasing priority. To complete a mission within a reasonable time frame, even to the nearest extra-solar system objects of interest, the Oort Cloud or the Alpha Centauri star system (4.3 light years away), the velocity of the spacecraft needs to be high, up to more than 10% of the speed of light. To achieve such speed one needs the highest energy-density fuel conceivable. This fuel would be antimatter, a large amount of it and in a compact form.

[1] Email addresses: mmn@lanl.gov, michael.holzscheiter@cern.ch, turyshev@jpl.nasa.gov

Antimatter can produce three orders-of-magnitude more energy per gram than fission or fusion and ten orders-of-magnitude more energy per gram than the chemical reactions currently used for propulsion. As a result, antimatter is a prime candidate for use in future exploration beyond the solar system. It also is a candidate for future missions to the edge of the solar system, that now require 15-20 years after launch just to reach Pluto.

In this talk (MMN) we start with a quick review of both the discovery of antimatter and also our understanding of antimatter (Section 2). In Section 3 a description is given of how cold antihydrogen was created at CERN in 2002. We point out why this is the only form of antimatter that is practical for deep space propulsion. We then take a side trip into current studies using antiprotons for cancer therapy (Section 4). This side trip is important because medical research may help with the justification for funding necessary to yield large amounts of antimatter. In Section 5 we outline the trail we need to break to obtain the dense antihydrogen that would be needed for deep space travel. We go on in Section 6 with a discussion of what we can do now to start on this path, providing a roadmap towards the goal. Our conclusions follow.

# 2 History of Antimatter

It turns out that, given quantum mechanics and special relativity, antimatter's existence is a consequence [1]-[4]. Although there are hints of the possible existence of antimatter in the *strong reflection* solutions of special-relativity, the complete break-though came after Dirac discovered his relativistic equation for the hydrogen atom [5], whose solutions precisely agreed with the observed energy levels.

That is, this equation had four solutions, which could be interpreted as those for particles with energy and internal spin properties

$$\Psi_{Dirac} \sim \{+E \text{ spin up}, \ +E \text{ spin down}, \ -E \text{ spin down}, \ -E \text{ spin up}\}. \qquad (1)$$

But the last two solutions had *negative energies*. This led to a huge controversy which was only resolved when Anderson discovered the positron in 1932 [6, 7]. This is a(n) (anti)particle with the same mass as, but opposite electric charge as, the electron.

Over the years, the antiproton, the antineutron, and, indeed with the development of modern particle accelerators, all possible forms of antimatter that can be detected have been detected. We have come to understand antimatter theoretically in terms of the $CPT$-theorem of modern field theory.

In an intuitive form, the theorem says that if one were to take a motion picture of a physical process and if one then were to change the "charges" or "internal quantum numbers" of the particles in the movie ($C$), run the film backwards ($T$), and look at it in a mirror after rotating oneself by 180° then one would not be able to tell the difference in the laws of physics being seen. Put another way, this theorem states that every particle has an antiparticle with

i) the opposite electric charge,

ii) the opposite internal quantum numbers,

iii) the opposite magnetic moment,

iv) the same total lifetime, and

v) the same (inertial) mass.

Although active searches continue for violations of this theorem, none has been found.

Most importantly for us, if a particle and an antiparticle collide they annihilate each other. For example, if a positron hits an electron, they turn into two high-energy gamma rays, each of energy of the rest mass of one particle, 511 keV. Stored antimatter would be, by definition, the most powerful battery per unit mass ever created.

Positrons (antielectrons) are now easily created in the laboratory from $^{22}$Na sources and controlled in Penning traps [8]. With much more difficulty (an efficiency of 1 part in $10^{10}$) antiprotons are created in high-energy accelerators. At CERN in Geneva, Switzerland, these antiprotons have been (again inefficiently) cooled and stored in Penning traps for fundamental physics experiments.

However, these particles are by themselves not viable for antimatter propulsion. The storage volume must be small. Charged antimatter is limited by the Brillouin density [9]

$$n_0 = \frac{B^2}{2\mu_0 mc^2}. \tag{2}$$

For antiprotons stored in a magnetic field using today's technology, say fields of 6 T or even 25 T, this density would be around $10^{11}$ or $2 \times 10^{12}$ cm$^{-3}$, respectively. (This number is itself many orders-of-magnitude higher than the highest antiproton density so far achieved, $\sim 10^6$ cm$^{-3}$ [10, 11].) Thus, charged antimatter is ruled out. This leaves stable, neutral antimatter, i.e., antihydrogen, for a fuel candidate.

Since, as we come to in the next section, cold antihydrogen has now been produced in the laboratory, it has been argued [12] that a fundamental science program needs to be undertaken to manufacture and control dense antihydrogen, first in the form of a cold dense gas or even a Bose-Einstein Condensate. The long range goal is eventually to obtain condensed antihydrogen, either as a molecular superfluid, a cluster ion, or as a diamagnetic solid. This accomplishment would allow a compact source of antimatter to be used for deep-space propulsion. But, as many have argued, its use would be tremendously powerful [13].

# 3 How Cold Antihydrogen was Created (2002)

Since positrons and antiprotons both have been produced, then clearly antihydrogen should also be able to be made. But it was not so easy. Until recently, only a few atoms of antihydrogen had been produced at CERN [14] and at Fermilab [15] in high energy collisions. But these antiatoms were produced at relativistic speeds, much too fast to capture and study. But in late 2002, the ATHENA collaboration announced it had produced the first low-energy antihydrogen atoms (50,000 of initially, later more) [16], using antiprotons contained in a

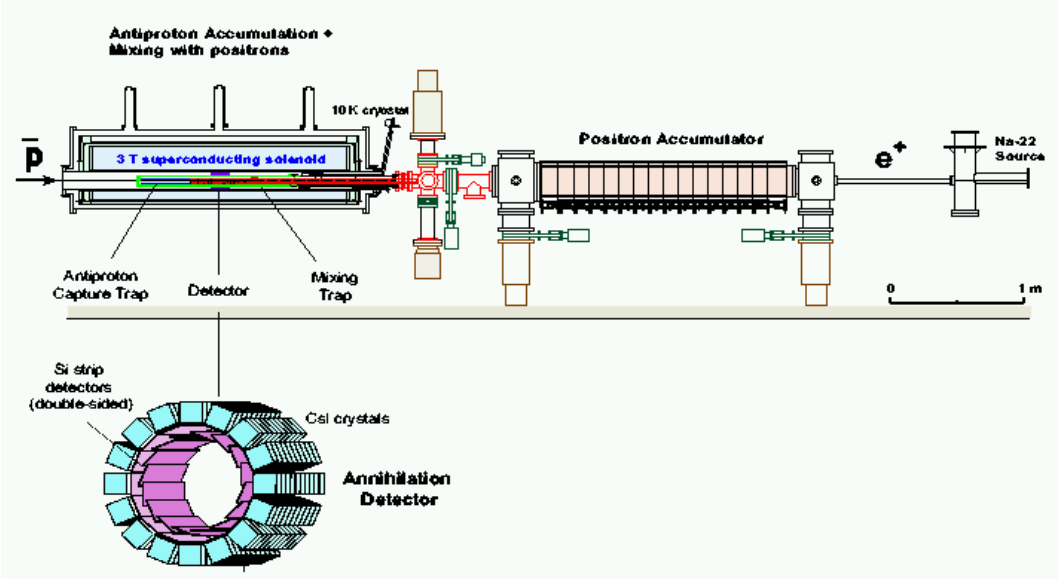


Figure 1: General lay-out of the ATHENA experiment [18]. Shown are the positron accumulator and the main magnet system holding the antiproton catching trap, the final positron storage trap, and the recombination region. The antihydrogen detector surrounds the trap.

Penning trap after having been extracted from the AD (Antiproton Decelerator) at CERN. The excitement this produced was magnified by coverage in the international press [17].

The general lay-out of the ATHENA experiment is shown in Figure 1. The central portion of the ATHENA apparatus is shown schematically in Figure 2(a), whilst the relevant trap potentials are illustrated in Figure 2(b).

In each antiproton beam extraction, about $10^4$ antiprotons are mixed with about $10^8$ positrons. Once the low-energy antihydrogen atoms are produced, they are neutral and no longer are bound in the Penning trap configuration. This are free to wander in the direction of their momentum after creation. They annihilate with normal once they collide with any, which is preferentially at the walls of the trap. The signal of an event is the simultaneous (within 1 $\mu$s) detection of (i) two back-to-back 511 keV gamma rays (from the positron annihilating with an electron) and (ii) about three charged pions (from the antiproton annihilating with a nucleon) with the pions' momenta directions all converging backwards to a single vertex point (to within a few mm) which is on the line of the emitted photons.

In Figure 3 we show the verification of the creation of antihydrogen by the detection of the annihilation products, seen to be preferentially at the walls of the trap.

Shortly after the ATHENA discovery, the ATRAP experiment also announced antihydrogen production [19, 20]. It is now the goal of these collaborations working at the AD to cool these antihydrogen atoms even further, to confine them possibly in a magnetic trap, and to perform experiments with them.

This production and storage of neutral antihydrogen completed a major step on the road

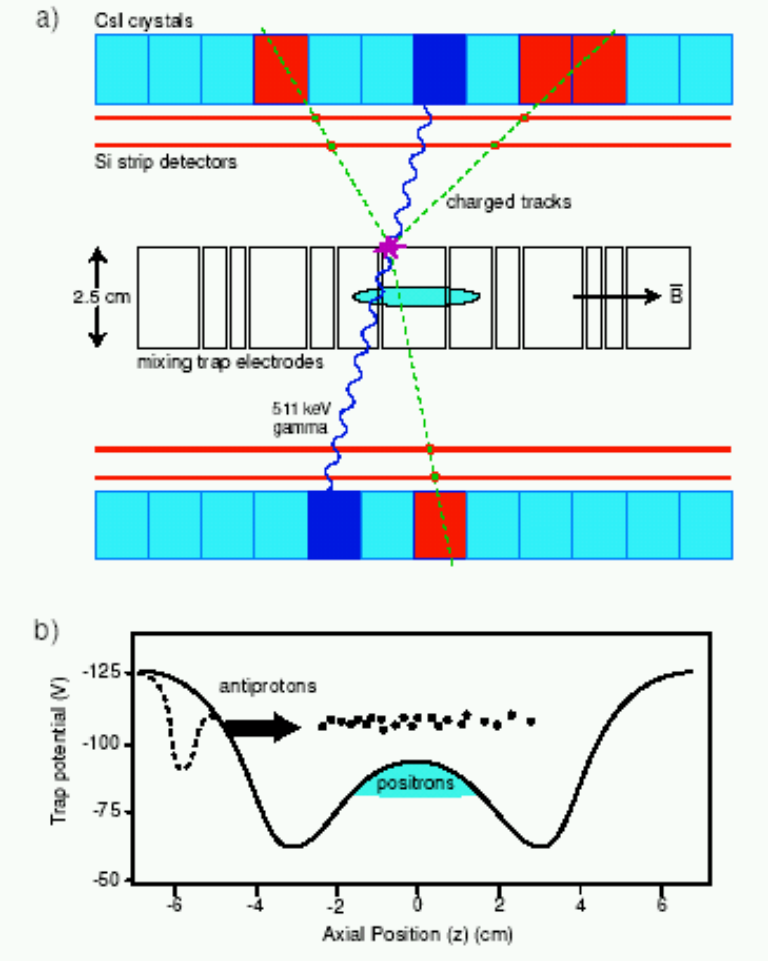


Figure 2: Schematic of the central portion of the ATHENA apparatus and the trapping potential used [16]. (a) Section of the mixing trap and detector showing the cylindrical electrodes and the position of the positron cloud. A typical antihydrogen annihilation event with the emission of three charged pions and a pair of back-to-back 511 keV gamma-rays is shown. (b) The trapping potential on axis is plotted along the length of the trap. The dashed line shows the potential before the antiprotons and positrons are mixed.

to the technology we are envisioning for antimatter deep-space propulsion.

# 4 Not-really-a-side-bar: Antiproton Cancer Therapy

Simultaneously with the antihydrogen experiments at CERN, the low-energy antiproton beam from the AD was being used by the AD-4 collaboration to study the effect of antiprotons on living tissue as a precursor to possible cancer therapy. An advantage of antiprotons over protons or heavy ions is expected from the extra burst of annihilation energy deposited at the stopping point (Bragg Peak). By proper choice of the beam energy this point can be located precisely inside the tumor volume, which would give a higher proportion of destruc-

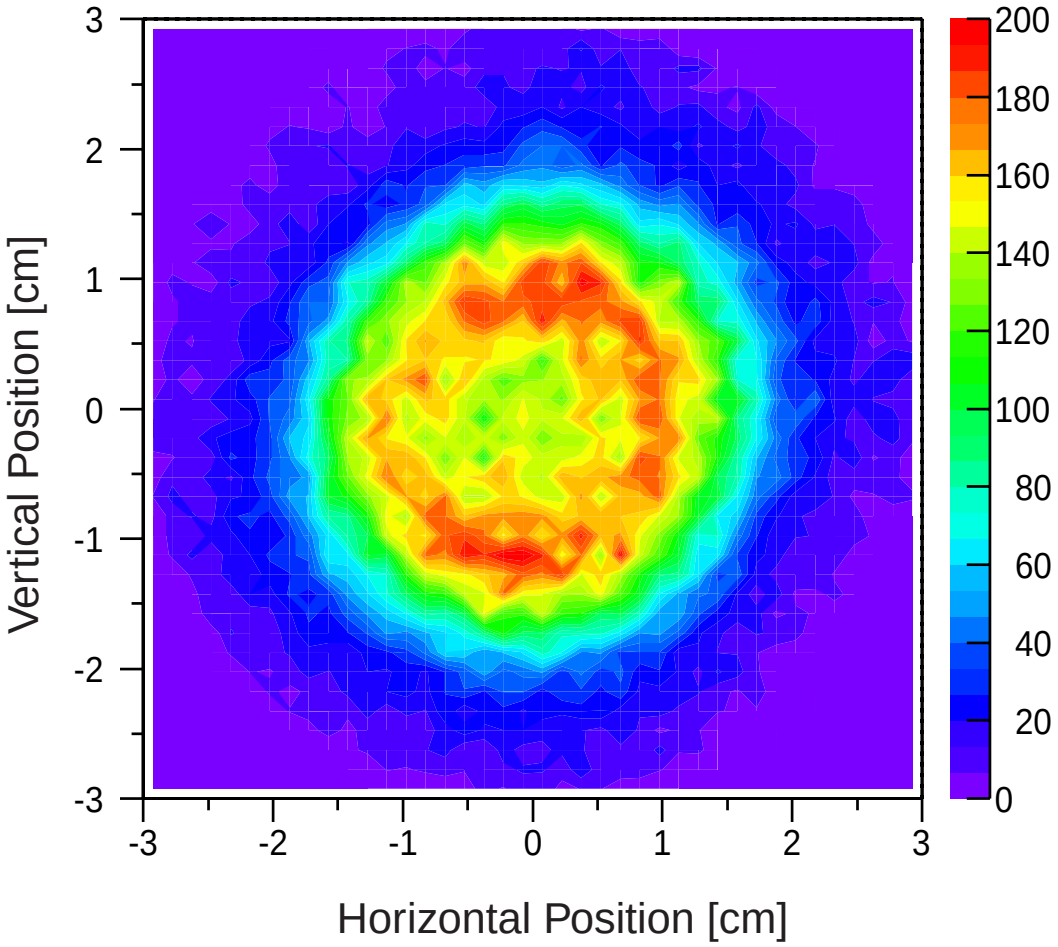


Figure 3: Contour plot of the distribution (obtained by projecting onto the plane perpendicular to the magnetic field) of the vertex positions of reconstructed antihydrogen annihilation events from the ATHENA cold antihydrogen production experiment [16].

tion to the cancer cells vs. the normal tissue the beam went through.

Preliminary results indicate this enhancement is true [21] and also that perhaps as few as $10^{10}$ antiprotons could treat a tumor of size about 1 $cm^3$ [22]. Since present accelerators, such as the former AC/AA combination at CERN or the future facility at GSI, produce on the order of $10^{14}$ antiprotons/year, this therapy application has entered the realm of being a realistic possibility. State-of-the-art modifications to current accelerator designs could possibly produce a factor 10-100 more antiprotons.

Such production would make antiproton therapy realizable, and the funds to produce such a source might be reasonably requested from the NIH. As emphasized in Section 6.1,this mutual benefit could lead to a symbiotic funding partnership with NASA. Indeed, discussions to pursue such a source for therapy purposes are already under way.[2]

[2]A straw-man design is currently being studied by the AD-4 collaboration [21].

# 5 The Route to Dense Antihydrogen and Deep Space Travel

Long-term storage of substantial amounts of antimatter must be developed to enable space missions relying on antimatter-based propulsion systems. Although it is clear that ultimately neutral antimatter must be used, up to now, no valid long-term storage concept for large quantities of antihydrogen has been developed. On the other hand, now that cold antihydrogen has been created, the next steps are to capture it and to cool it even further. Designs for the first goal are now being developed at CERN. They concentrate on being able to build a trap that confines the plasmas before combination and yet also confines the neutral antihydrogen afterwards.

This confinement would be accomplished by surrounding the Penning trap configuration with a magnetic quadrupole configuration, yielding a magnetic field

$$\mathbf{B} = B_0 \left[ \hat{\mathbf{z}} + \frac{(x\hat{\mathbf{x}} - y\hat{\mathbf{y}})}{R_0} \right]. \tag{3}$$

with a minimum at its center. One would then use the magnetic dipole force on the antihydrogen atom

$$\mathbf{F}_{mag} = \mu \cdot \nabla \mathbf{B} \tag{4}$$

to trap the atoms in the so-called "low-field seeking states." (The upper two states in the hyperfine diagram for the ground state of atomic hydrogen.)

If this difficult work succeeds (and there appear to be no matter-of-principle problems with it) the next goal will be to cool the captured antihydrogen atoms to very low temperatures, perhaps using the Lyman-alpha lasers that are being developed.

The first step in producing dense antihydrogen would be to produce what has been done for hydrogen atoms, a Bose-Einstein Condensate (BEC).[3] BEC confinement of neutral spin-polarized hydrogen atoms at densities up to $5 \times 10^{15}$ cm$^{-3}$ has been demonstrated. [23], which is orders-of-magnitude more dense than the Brillouin storage density limit for charged antiprotons. To make a BEC of antihydrogen would be an important step where one could learn the techniques of controlling a relatively large amount of antihydrogen. One also would need to overcome the problem of the antihydrogen transitioning out of the confined states [12]. The clear ultimate goal would be to make very dense antihydrogen in the form of clusters or solids (perhaps stored diamagnetically).

At present the wasteful method of resonant evaporative cooling is used to achieve the temperatures and densities needed to form a hydrogen BEC. But the development of lasers for direct and efficient cooling of hydrogen atoms has now just started. Efficient laser cooling of hydrogen will revolutionize the methodology of forming, controlling, and studying hydrogen Bose-Einstein Condensates. These studies can all be done with ordinary matter, in preparation for having more copious amounts of antihydrogen available.

If the envisioned progress comes to fruition, laser cooling could then be used in an attempt to efficiently make an antihydrogen BEC. An antihydrogen BEC would be an impor-

[3] A BEC is a gaseous coherent quantum system, just as are superfluid helium or superconducting currents.

tant step down a path that could eventually lead to even more dense antihydrogen molecules, liquids, solids, and cluster ions [24]-[26]. Indeed, since one might expect the next stage to be going from controlled ultra-cold (below 50 $\mu$K) BEC hydrogen atoms to controlled hydrogen molecules, it is heartening that there is evidence of a hydrogen-molecule superfluid with a critical temperature of 0.15 K [27]. Since the triple point of hydrogen is at 13.8 K, a potential path to denser condensed antimatter becomes more interesting.

# 6 What Can We Do Now?

A space-certified storage system for neutral antimatter will not be obtained from a linear extrapolation of heretofore existing technologies. Rather, this achievement requires a series of scientific and/or technological breakthroughs. While breakthroughs can never be predicted, they typically will not happen without the definition of a strong need and the challenge presented to the scientific community by a truly ambitious goal.

Meanwhile many of the underlying issues can be addressed with both the modest supply of antimatter available at this time at accelerator centers world wide and with the limited means to store the particles. The technological and scientific knowledge gained in these tests will enable us to lay out a path into the future of antimatter-based propulsion systems.

However, the most important item is the need for a dedicated low-energy antiproton source in the United States.

## 6.1 A dedicated Low-Energy Antiproton Source in the USA

The biggest obstacle to producing copious antihydrogen in the U.S. is the dearth of low-energy antiproton production here . As stated, antiproton production presently is a very inefficient process and is done only in Europe. At present the only source of low-energy antiprotons is at CERN. It is hoped that the AD facility at CERN will keep running until perhaps the end of this decade. Then a newly proposed facility, FLAIR (A facility for Low-energy Antiproton and Ion Research), will hopefully be built at the GSI accelerator center in Germany. FLAIR could yield $10^{12}$ *low energy* antiprotons per year.

But the US needs a facility so it can realistically pursue the ultimate goal of copious production of antiprotons leading to copious antihydrogen. It is only with a viable facility that studies can be done that will lead to the necessary break-through technology needed for more efficient antiproton production.

The communities to accomplish this, perhaps as a consortium, are there. The DOE physics community would like such a facility to continue fundamental symmetry studies on antimatter and also to test gravity [4]. As pointed out in Section 4, the work on antiproton therapy would lead to NIH interest in this facility. NASA would have an interest for deep-space flight. There are also other communities that would have an interest: space reactor teams, RTG builders, radiation physicians and physicists, and nuclear and particle experimentalists. A NASA/DOE/NIH consortium to build a dedicated facility would be a natural.

## 6.2 A Roadmap to Antihydrogen Propulsion

Knowing the cost of acquiring the technological capabilities needed to produce large quantities of antihydrogen atoms, to store them for long periods, and to use them for propulsion purposes in space is, of course, very important. Given our present technological level, our estimates are that:

• It would take about 5-10 years and ~$0.5-1.0 B to build a source.

• It would take about the same additional time and money to develop antihydrogen handling technologies.

During all this time, effort would be given to developing the new antiproton production technology that is needed. Current antiproton production rates are low. While clever techniques can enhance these rates by several orders-of-magnitude and quantities sufficient for advanced concepts can be produced given enough economic and political pressure onto the few available sources, a real breakthrough can only come through continued interest and research in this area. A good analogy is the comparison between a light bulb and a laser. In both cases light is produced, but in one system through thermal heating of a material and in the other through coherent processes. Antiprotons are currently produced by heating a metal target with a primary proton beam. This process is a direct analogy to the light bulb — we are still awaiting the invention of a 'laser-equivalent' for the production of particles of antimatter.

• A GUESS is that 10-20 years more would be needed for this new process to be developed.

Development of the new, more efficient process would be the make or break point. If after 30 years one did not have a new antiproton production technology, then the effort would be abandoned as far as deep-space propulsion is concerned, although not for the other applications. But with success,

• A BIGGER GUESS is that it would take 10-20 more years to develop a real propulsion system.

Note that much of the technology will be standard in the sense that the power transfer from antimatter annihilation to thrust has long been a problem of interest [3, 28], similar to that of obtaining thrust from other nuclear mechanisms [29, 30].

So, we are talking of about $50 billion over 50 years. That period is like the time it took to advance from vacuum-tube computers to the microchip processors of today. It would be a viable time frame - if it works. But most importantly, antimatter science has now advanced to the point where antimatter technology has left the realm of science fiction and has reached the first stages of reality.[4]

[4]Indeed, if one considered positron emission tomography (PET), the reality arrived some time ago.

# 7 Conclusions

The road we have described is challenging both scientifically and technologically. Enormous scientific and technological barriers must be overcome. But the potential intellectual and societal rewards, even along the way, are enormous.

Antimatter-matter annihilation is one of the prime candidates to achieve the high specific impulse i) desired for the challenging missions of exploring the Heliopause and visiting the Oort Cloud, and ii) needed if we plan to attempt a rendezvous with the nearest star systems. While no clear pathway to the necessary technologies exists, experimental development in the normal matter world of laboratory-sized research equipment can help us to reach these most ambitious goals, *IF* we simultaneously embark on constructing a dedicated low-energy antiproton facility

It behooves us to now embark on extensive, serious work on the possibilities that are before us. To achieve them quickly it is necessary to set ourselves in motion now.

# Acknowledgements

MMN and MHH acknowledge the support of the United States Department of Energy, partially under contract W-7405-ENG-36 (MMN). The work of SGT was performed at the Jet Propulsion Laboratory, California Institute of Technology, under contract with the National Aeronautics and Space Administration.

# References

[1] R. P. Feynman, in: *Elementary Particles and the Laws of Physics. The 1988 Dirac Memorial Lectures* (Cambridge Univ. Press, Cambridge, 1987).

[2] M. M. Nieto and R. J. Hughes, "Antimatter: Its History and its Properties," in: [3], p. 228.

[3] B. W. Augenstein, B. E. Bonner, F. E. Mills, and M. M. Nieto, eds, *Antiproton Science and Technology* (World Scientific, Singapore, 1988). See, especially, Group. III Papers, "Applied Science and Technology."

[4] M. H. Holzscheiter, M. Charlton, and M. M. Nieto, "The Route to Ultra Low-Energy Antihydrogen," Phys. Rep. 402 (2004) 1.

[5] P. A. M. Dirac, "The Quantum Theory of the Electron," Proc. Roy. Soc. A 117 (1928) 610.

[6] C. D. Anderson, "The Apparent Existence of Easily Deflectable Positives," Science 76 (1932) 238.

[7] C. D. Anderson, "The Positive Electron," Phys. Rev. 43 (1933) 491.

[8] H. Dehmelt, "Experiments with an Isolated Subatomic Particle at Rest," Rev. Mod. Phys. 62 (1990) 525.

[9] L. Brillouin, "A Theorem of Lamour and Its Importance for Electrons in Magnetic Fields," Phys. Rev. 67 (1967) 260.

[10] M. H. Holzscheiter. X. Feng, T. Goldman, N. S. P. King, R. A. Lewis, M. M. Nieto, and G. A. Smith, "Are Antiprotons Forever?" Phys. Lett. A 214 (1996) 279.

[11] M. M. Nieto and M. H. Holzscheiter, "A Catching Trapp for All Antiproton Seasons," Appl. Phys. B 60 (1995) 103.

[12] M. M. Nieto, M. H. Holzscheiter, and T. J. Phillips, "Dense Antihydrogen: Its Production and Storage to Envision Antimatter Propulsion," J. Optics B: Quant. Semiclass. Optics 5 (2003) S547.

[13] G. Genta, "Propulsion for Interstellar Space Exploration," in: *Outer Heliosphere: The Next Frontiers*, Cospar Colloquium Series, 11, eds. K. Scherer, H. Fichtner, H. J. Fahr, and E. Marsch (Elsevier Science, Amsterdam, 2001), p. 421.

[14] G. Baur, G. Boero, S. Brauksiepe, A. Buzzo, W. Eyrich, R. Geyer, D. Grzonka, J. Hauffe, K. Kilian, M. Lo Vetere, M. Macri, M. Moosburger, R. Nellen, W. Oelert, S. Passaggio, A. Pozzo, K. Róhrich, K. Sachs, G. Schepers, T. Sefzick, R. S. Simon, R. Stratmann, F. Stinzing, and M. Wolke, "Production of Antihydrogen," Phys. Lett. B, 368 (1996) 251.

[15] G. Blanford, D. C. Christian, K. Gollwitzer, M. Mandelkern, C. T. Munger, J. Schultz and G. Zioulas, "Observation of Atomic Antihydrogen," Phys. Rev. Lett. 80 (1998) 3037.

[16] M. Amoretti, C. Amsler, G. Bonomi, A. Bouchta, P. Bowe, C. Carraro, C. L. Cesar, M. Charlton, M. J. T. Collier, M. Doser, V. Filippini, K. S. Fine, A. Fontana, M. C. Fujiwara, R. Funakoshi, P. Genova, J. S. Hangst, R. S. Hayano, M. H. Holzscheiter, L. V. Jørgensen, V. Lagomarsino, R. Landua, D. Lindelof, E. L. Rizzini, M. Macri, N. Madsen, G. Manuzio, M. Marchesotti, P. Montagna, H. Pruys, C. Regenfus, P. Riedler, J. Rochet, A. Rotondi, G. Rouleau, G. Testera, A. Variola, T. L. Watson, and D. P. van der Werf, "Production and Detection of Cold Antihydrogen Atoms," Nature 419 (2002) 456.

[17] http://athenA-positrons.web.cern.ch/ATHENA-positrons/wwwathena/inthenews.html

[18] M. Amoretti, C. Amsler, G. Bonomi, A. Bouchta, P. D. Bowe, C. Carraro, M. Charlton, M. J. T. Collier, M. Doser, V. Filippini, K. S. Fine, A. Fontana, M. C. Fujiwara, R. Funakoshi, P. Genova, A. Glauser, D. Grögler, J. S. Hangst, R. S. Hayano, H. Higaki, M. H. Holzscheiter, W. Joffrain, L. V. Jørgensen, V. Lagomarsino, R. Landua, C. Lenz Cesar, D. Lindelöf, E. Lodi Rizzini, M. Macrí, N. Madsen, G. Manuzio, P. Montagna, H. Pruys, C. Regenfus, P. Riedler, J. Rochet, A. Rotondi, G. Rouleau, G. Testera, D. P. van der Werf, A. Variola, T. L. Watson, T. Yamazaki, and Y. Yamazaki, "The

ATHENA Antihydrogen Apparatus," Nucl. Instru. and Meth. Phys. Res. A 518 (2004) 679.

[19] G. Gabrielse, N. S. Bowden, P. Oxley, A. Speck, C. H. Storry, J. N. Tan, M. Wessels, D. Grzonka, W. Oelert, G. Schepers, T. Sefzick, J. Walz, H. Pittner, T. W. Hänsch, and E. A. Hessels, "Background-Free Observation of Cold Antihydrogen with Field-Ionization Analysis of Its States," Phys. Rev. Lett. 89 (2002) 213401.

[20] G. Gabrielse, N. S. Bowden, P. Oxley, A. Speck, C. H. Storry, J. N. Tan, M. Wessels, D. Grzonka, W. Oelert, G. Schepers, T. Sefzick, J. Walz, H. Pittner, T. W. Hänsch, and E. A. Hessels, "Driven Production of Cold Antihydrogen and the First Measured Distribution of Antihydrogen States" Phys Rev. Lett. 89 (2002) 233401.

[21] C. Maggiore, N. Agazaryan, N. Bassler, E. Blackmore, G. Beyer, J. J. DeMarco, M. Doser, C. R. Gruhn, M. H. Holzscheiter, T. Ichioka, K. S. Iwamoto, H. V. Knudsen, R. Landua, W. H. McBride, S. P. Møller, J. Petersen, J. B. Smathers, L. D. Skarsgard, T. D. Solberg, U. I. Uggerhøj, H. R. Withers, and B. G. Wouters, "Biological Effectiveness of Antiproton Annihilation," Nucl. Instru and Meth. Phys. Res. B 214 (2004) 181.

[22] AD-4 collaboration, unpublished.

[23] D. G. Fried, T. C. Killian, L. Willmann, D. Landhuis, S. C. Moss, D. Kleppner, and T. Greytak, "Bose-Einstein Condensation of Atomic Hydrogen," Phys. Rev. Lett. 81 (1998) 3811.

[24] I. F. Silvera, "The Solid Molecular Hydrogens in the Condensed Phase: Fundamentals and Static Properties," Rev. Mod. Phys. 52 (1980) 393.

[25] W. C. Stwalley, "The Synthesis of large Cluster Ions from Elementary Constituents," in: [3], p. 373.

[26] D. A. Young, *Phase Diagrams of the Elements*, (Berkeley: University of California Press, Berkeley, 1991) Chap. 4.

[27] S. Grebenev, B. Sartakov, J. P. Toennies, and A. F. Villesov, "Evidence for Superfulidity in Para-hydrogen Clusters Inside Helium-4 Droplets at 0.15 Kelvin," Science 289 (2000) 1532.

[28] R. L. Forward, "Antiproton Annihilation Propulsion", Air Force Rocket Propulsion Laboratory report AFRPL TR-85-034 (1985).

[29] T. Kammash, "Antiproton Driven Magnetically Insulated Inertial Confinement Fusion (MICF) Propulsion System," NIAC 98-02 Final Report (1998), available at `http://peaches.niac.usra.edu/studies/study_master.jsp?action=Call`

[30] R. A. Lewis, G. A. Smith, E. Cardiff, B. Dundore, J. Fulmer, B. J. Watson, and S. Chakrabarti, "Antiproton-Catalyzed Microfission/Fusion Space Propulsion Systems for the Exploration of the Outer Solar System and Beyond," in: Space Technology and Applications International Forum. (STAIF-97), ed. M. S.El-Genk, AIP Conference Proceedings No. 387, Pt. 3, (American Institute of Physics, NY, 1997), p. 1499.